

Legionella maintains host ubiquitin homeostasis by effectors with unique catalytic mechanisms

Zhao-Qing Luo

luoz@purdue.edu

Purdue University West Lafayette <https://orcid.org/0000-0001-8890-6621>

Jiaqi Fu

The First Hospital of Jilin University <https://orcid.org/0000-0003-0081-6133>

Siyang Li

The First Hospital of Jilin University

Wei Xian

Peking University Health Science Center <https://orcid.org/0000-0002-3683-7983>

Zhengrui Zhang

Purdue University

Tao-Tao Chen

College of Life Sciences, Fujian Normal University <https://orcid.org/0000-0002-0660-2841>

Yao Liu

Purdue University <https://orcid.org/0000-0002-4330-2389>

Qihua Lu

Fujian Normal University

Songying Ouyang

Fujian Normal University <https://orcid.org/0000-0002-1120-1524>

Chittaranjan Das

Purdue University West Lafayette <https://orcid.org/0000-0002-0567-7753>

Xiaoyun Liu

Peking University Health Science Center <https://orcid.org/0000-0001-7083-5263>

Lei Song

The First Hospital of Jilin University

Hongxin Guan

Fujian Normal University

Chuang Li

Purdue University West Lafayette

Qingtian Guan

First Hospital of Jilin University

Jingting Wang

Fujian Normal University

Jinyu Li

Fuzhou University <https://orcid.org/0000-0002-8220-049X>

Lina Kang

Fujian Normal University

Si-Ru Zheng

Fujian Normal University

Shoujing Cao

Fuzhou University

Article

Keywords: Adenylation, posttranslational modification, ubiquitination, bacterial toxins

Posted Date: May 20th, 2024

DOI: <https://doi.org/10.21203/rs.3.rs-4431542/v1>

License:   This work is licensed under a Creative Commons Attribution 4.0 International License.

[Read Full License](#)

Additional Declarations: There is **NO** Competing Interest.

27 **Summary**

28 The reversal of ubiquitination induced by members of the SidE effector family of
29 *Legionella pneumophila* produces phosphoribosyl ubiquitin (PR-Ub) that is potentially
30 detrimental to host cells. Here we show that the effector LnaB functions to transfer the
31 AMP moiety from ATP to the phosphoryl moiety of PR-Ub to convert it into ADP-
32 ribosylated ubiquitin (ADPR-Ub), which is further processed to ADP-ribose and functional
33 ubiquitin by the (ADP-ribosyl)hydrolase MavL, thus maintaining ubiquitin homeostasis in
34 infected cells. Upon being activated by Actin, LnaB also undergoes self-AMPylation on
35 tyrosine residues. The activity of LnaB requires a motif consisting of Ser, His and Glu (S-
36 HxxxE) present in a large family of toxins from diverse bacterial pathogens. Our study not
37 only reveals intricate mechanisms for a pathogen to maintain ubiquitin homeostasis but
38 also identifies a new family of enzymes capable of protein AMPylation, suggesting that
39 this posttranslational modification is widely used in signaling during host-pathogen
40 interactions.

41

42 Key words: Adenylylation, posttranslational modification, ubiquitination, bacterial toxins

43

44 **Introduction**

45 Successful pathogens use virulence factors to actively modulate host processes
46 to evade cell-autonomous defense and immune detection. It is now recognized that the
47 activity of virulence factors is a double-edged sword for the pathogen: on one hand, these
48 factors are essential for colonizing their hosts; on the other hand, cellular damage inflicted
49 by pathogenic factors can be detected by specific receptors, leading to robust immune
50 responses ¹. To minimize the chance of virulence factors being used as immune agonists,
51 pathogens have evolved various regulatory mechanisms, including tight regulation of
52 gene expression, precise targeting to specific cellular compartments and/or the use of
53 additional virulence factors to dampen the immune response ²⁻⁴.

54 In some scenarios, virulence factors may disrupt host cell homeostasis, thus
55 making the cell less suitable for pathogen replication. One such example is the
56 intracellular bacterial pathogen *Legionella pneumophila*. This bacterium creates an
57 intracellular niche permissive for its replication utilizing a large cohort of effectors to
58 modulate host processes by diverse biochemical activities ⁵. Among the scores of
59 effectors that target the ubiquitin network, members of the SidE effector family pose
60 unique challenges to host cells. These effectors catalyze protein ubiquitination by a
61 mechanism involving the production of ADP-ribosylated ubiquitin (ADPR-Ub) as the
62 reaction intermediate using their monoADP-ribosyltransferase (mART) activity ⁶. ADPR-
63 Ub is then used to modify substrate proteins by their phosphodiesterase (PDE) domains
64 ^{7,8}. These two reactions are uncoupled, ADPR-Ub may accidentally release into the
65 cytosol of infected cells. Furthermore, the reversal of SidEs-induced ubiquitination by
66 DupA and DupB produces phosphoribosyl ubiquitin (PR-Ub) ^{9,10}. Neither ADPR-Ub nor
67 PR-Ub can be used in canonical ubiquitination reactions ⁷, and their accumulation may
68 interfere with key signaling cascades in infected cells and ultimately impede bacterial
69 replication. These challenges necessitate mechanisms to maintain ubiquitin homeostasis
70 in infected cells.

71

72 **Results**

73 **The macro domain protein MavL is an (ADP-ribosyl)hydrolase against ADPR-Ub**

74 We attempted to identify additional *L. pneumophila* effectors involved in ubiquitin
75 signaling using biotin-mediated proximal labeling (Turbo ID) ¹¹, the BirA*-Ub fusion (BirA*,

76 the promiscuous BirA mutant)¹¹ was expressed in *L. pneumophila* and biotinylated
77 proteins were identified by mass spectrometry (**Fig. S1a**). Not surprisingly, a number of
78 Dot/Icm effectors known to be involved in ubiquitin signaling were identified. In addition,
79 a few effectors of unknown function were detected with high confidence (**Fig. S1b**).
80 Among these, MavL(Lpg2526) has been studied in a recent study which reveals that this
81 protein binds ADP-ribose and structural overlay with poly-(ADP-ribose) glycohydrolases
82 (PARGs) identified two aspartate residues potentially involved in catalysis¹². This study
83 also found that MavL interacts with the mammalian ubiquitin-conjugating enzyme
84 UBE2Q1, suggesting a role in ubiquitin signaling¹². In light of these observations and the
85 fact MavL was identified in our screening strategy based on ubiquitin interaction, we
86 further pursued the hypothesis that MavL acts on proteins that have been modified by
87 ubiquitination, ADP-ribosylation or both. That ADPR-Ub is inactive in canonical
88 ubiquitination reactions (Supplementary **Fig. 1c**) prompted us to examine whether it is a
89 substrate of MavL. Indeed, recombinant MavL effectively hydrolyzed ADPR-Ub into
90 ADPR and ubiquitin, which is in contrast to DupA and DupB (**Fig. 1a**). Like most Dot/Icm
91 effectors, MavL is not required for bacterial intracellular growth (Supplementary **Fig. 1d**).
92

93 To understand the catalytic mechanism of the ADP-ribosylhydrolase (ARH) activity
94 of MavL, we screened its active truncation mutants and succeeded in solving the structure
95 of the MavL₄₀₋₄₀₄-ADPR complex at a resolution of 2.38 Å, which revealed that several
96 pairs of hydrogen bonds and a π-π stacking interaction provided by surrounding amino
97 acids or water molecules are involved in interactions between MavL and ADPR
98 (Supplementary **Fig. 1e**). The negatively charged residues D315, D323 and D333 likely
99 form a catalytic loop (β8-α8) that directly interacts with the hydroxyl groups of ribose by
100 hydrogen bonding (Supplementary **Fig. 2a**). Mutational analysis indicated that all three
101 residues are critical for the ARH activity of MavL against ADPR-Ub (**Fig. 1b**). The role of
102 D323 and D333 in catalysis has been predicted in an earlier structural study of MavL¹².
103 Furthermore, the mutants MavL_{D315A} and MavL_{D323A} displayed higher affinity toward
104 ADPR-Ub and ADPR (**Fig. 1c**, Supplementary **Fig. 2b**, **Fig. 3** and **Fig. 4**). Further efforts
105 using these mutants allowed us to obtain the structure of the MavL₄₀₋₄₀₄(D315A)-ADPR-Ub
106 complex at a 1.93 Å resolution (**Fig. 1d, left**). The combined surface area of the interface
107 between MavL and ubiquitin is approximately 867.6 Å². In the complex, ADPR-Ub

108 engages MavL in such a way that the ADPR moiety linked to the side chain of R42 of
109 ubiquitin is inserted into the active-site pocket and the binding is coordinated by several
110 pairs of hydrogen bonds provided by G223, G225, C226, F227, K236, P264, N322, D323,
111 T331, D332, and D333 of MavL with D39 and R42 of ubiquitin (Supplementary **Fig. 2c**).
112 E107 and D323 of MavL hold R42 of ubiquitin in a position suitable for catalysis via
113 hydrogen bond interactions (**Fig. 1d, middle**). In addition, the side chain of D323 points
114 to the 1''-OH of the ADPR moiety and the -NH₂ of R42 in ubiquitin at a distance of 2.65
115 Å and 2.69 Å, respectively, thus is most likely the residue key for catalysis (**Fig. 1d,**
116 **middle**). Unexpectedly, the N-glycosidic bond between ADPR and R42 of ubiquitin was
117 cleaved in our structure, which may be caused by the residual activity of the D315A
118 mutant. (**Fig. 1d, right**).

119
120 Comparison of the structures of apo-MavL, MavL-ADPR, and MavL_{40-404(D315A)}-
121 ADPR-Ub revealed that the side chains of several residues, including F105, C226, Y232
122 and Q330 are involved in the formation of the activity pocket of apo-MavL that faces
123 outwards, keeping the binding pocket in an open state (**Fig. 1e**). Among these, the side
124 chains of C226 and Q330 form steric hindrance with the side chains of D39 and Q40 on
125 ubiquitin loop1 and E51 and D52 on ubiquitin loop2, respectively, preventing ubiquitin
126 from binding to apo-MavL (Supplementary **Fig. 5a**). Additionally, we observed four water
127 molecules around the ADPR moiety, two of which (H₂O-1 and H₂O-2) are also found in
128 other macro domain ARHs (Supplementary **Fig. 5b**). These two water molecules form a
129 hydrogen bond network with the α -phosphate of ADPR and the O1'' site of the distal
130 ribose group, wherein the α -phosphate activates H₂O-1 to initiate a nucleophilic attack on
131 the O1'' glycosidic bond, leading to its cleavage (**Fig. 1d, middle**).

132
133 We examined substrate specificity of MavL using several ADP-ribosylated proteins,
134 including ADPR-Ub_{T66} produced by CteC of *Chromobacterium violaceum*¹³, ADPR-Actin
135 induced by SpvB of *Salmonella enterica*¹⁴, ADPR-ANT1 catalyzed by Ceg3 of *L.*
136 *pneumophila*¹⁵, and ADPR-PARP1 catalyzed by Sirt6¹⁶. In addition to ADPR-Ub
137 produced by SidEs, ADP-ribosylhydrolysis against ADPR-ANT1 and ADPR-Actin also
138 detectably occurred (Supplementary **Fig. 2d**). We further examined the physiological role
139 of MavL by probing ADPR-Ub in cells infected with relevant *L. pneumophila* strains.

140 ADPR-Ub was detected in cells infected by wild-type *L. pneumophila* and its level was
141 elevated in samples infected with the $\Delta mavL$ mutant, and complementation with MavL but
142 not the inactive mutant MavL_{D323A} restored the phenotype (**Fig. 1f**), indicating that MavL
143 functions to reduce cellular ADPR-Ub. Our attempt to determine the distribution of MavL
144 in cells infected with *L. pneumophila* by immunostaining was not successful, probably due
145 to low protein abundance or the quality of our antibodies. Importantly, infection of cells
146 transfected to express HA-MavL revealed clear accumulation of protein on the Legionella-
147 containing vacuole (LCV) in a manner that required a functional Dot/Icm system
148 (Supplementary **Fig. 6**), suggesting that the effector mainly acts on the cytoplasmic
149 surface of the bacterial phagosome.

150

151 **The effector LnaB is an adenylyltransferase that converts PR-Ub into ADPR-Ub**

152 Efficient conversion of ADPR-Ub into ADPR and ubiquitin by MavL suggests that this
153 enzyme functions to return modified ubiquitin to its native form. Yet, MavL cannot remove
154 the phosphoribosyl group from PR-Ub (Supplementary **Fig. 2e**), we thus considered the
155 possibility that PR-Ub is first converted into ADPR-Ub prior to hydrolysis by MavL.

156

157 Dot/Icm effectors of relevant functions often are encoded by genes of close
158 proximity on the chromosome^{5,17}. The gene upstream of *mavL* is *mavK*(lpg2525), which
159 appears to harbor an F-box motif known to be involved in ubiquitination¹⁸. The genes
160 coding for LnaB (Lpg2527) and the deubiquitinase Lem27 (Lpg2529) (also known as LotC)
161¹⁹ are separated by a gene predicted to code for an α -amylase (Supplementary **Fig. 7a**).
162 We then examined the hypothetical proteins, MavK and LnaB, for the ability to convert
163 PR-Ub into ADPR-Ub. Incubation of recombinant MavK¹⁸ or LnaB with PR-Ub and ATP
164 did not detectably produce ADPR-Ub (Supplementary **Fig. 7b**). Some *L. pneumophila*
165 effectors are known to require host co-factors for their activity²⁰⁻²³, we thus added lysates
166 of mammalian cells to these reactions and found that native, but not heat-treated lysates
167 enabled LnaB to produce ADPR-Ub from PR-Ub (**Fig. 2a**). Thus, LnaB has the capacity
168 to convert PR-Ub into ADPR-Ub in the presence of a eukaryotic cell-specific molecule,
169 which likely is a protein due to its sensitivity to heat treatment.

170

171 To identify the host factor required for LnaB activity, we identified interacting
172 proteins by immunoprecipitation from lysates of cells transfected to express Flag-LnaB
173 by mass spectrometric analysis. Among the proteins specifically enriched by Flag-LnaB,
174 Actin was identified as the most differed and abundant hit (**Fig. 2b** and Supplementary
175 **Fig. 7c**). In line with these results, LnaB and Actin form a complex in cells that was readily
176 detectable by immunoprecipitation and by analytic ultracentrifugation (Supplementary **Fig.**
177 **7d-e**). ITC analysis revealed that these two proteins bind each other with a K_d of ~ 1.24
178 μM (**Fig. 2c**). More importantly, inclusion of Actin in reactions containing PR-Ub, ATP and
179 LnaB led to the production of ADPR-Ub (**Fig. 2d**). PR-Ub differs from ADPR-Ub only by
180 an adenosine monophosphate (AMP) moiety (**Fig. 2e**), suggesting that LnaB catalyzes a
181 reaction at the α phosphate center of ATP to transfer the AMP moiety onto PR-Ub. Indeed,
182 inclusion of ^{32}P - α -ATP in the reaction led to the production of radio-labeled ADPR-Ub,
183 again in an Actin-dependent manner (**Fig. 2f**).

184
185 ATP analogs containing a cleavable α phosphate, including adenylyl-
186 imidodiphosphate (AMPPNP) and adenosine 5'-(γ -thio)triphosphate (ATP γ S) supported
187 full activity of LnaB. In line with its partially susceptible α phosphate ²⁴, ATP α S also
188 supported the activity (**Fig. 2g**). In contrast, adenosine 5'-(α , β -methylene)triphosphate
189 (ApCpp), which has an uncleavable α -site, was unable to serve as the nucleotide donor
190 (**Fig. 2g**).

191
192 Similar results were obtained when the product of the reaction was analyzed by
193 mass spectrometry, which revealed that the tryptic peptide of ubiquitin (-
194 E₃₄GIPPDQQRLIFAGK₄₈-) derived from PR-Ub in which R42 was modified by
195 phosphoribosylation had been converted into ADP-ribosylation after incubation with ATP,
196 LnaB and Actin (**Fig. 3a-c**). Importantly, ADPR-Ub produced by LnaB from PR-Ub can be
197 used in ubiquitination induced by the PDE activity of SidEs. Incubation of the product with
198 SdeA_{E/A} (an SdeA mutant without mART activity but retaining its PDE function) led to
199 Rab33b ubiquitination at levels comparable to reactions receiving native ADPR-Ub (**Fig.**
200 **3d**). Furthermore, ubiquitin produced from PR-Ub by LnaB and MavL was active in
201 canonical ubiquitination reactions (**Fig. 3e**).

202

203 **LnaB utilizes an S-HxxxE motif to catalyze the conversion of PR-Ub into ADPR-Ub**

204 We explored the mechanism of action of LnaB using PSI-BLAST²⁵ searches to identify
205 proteins that may have common functional motifs, which revealed that LnaB belongs to a
206 family of toxins of at least 103 members that harbor a conserved S-HxxxE (x, any amino
207 acid) motif of unknown biochemical activity (Supplementary **Fig. 8**). Notably, the lengths
208 of the space between the conserved Serine and Histidine residues vary greatly among
209 members of the protein family (Supplementary **Fig. 8a**). These proteins are encoded by
210 diverse bacterial pathogens of a wide range of hosts, particularly a large set of proteins
211 categorized as Making caterpillar floppy (MCF) toxins found in insect pathogens
212 (Supplementary **Fig. 8b**)²⁶. Sequence alignment revealed that in LnaB, the S-HxxxE
213 motif is composed of S261, H305 and E309 (Supplementary **Fig. 8a**). We examined the
214 role of this predicted motif in the activity of LnaB by creating substitution mutants for each
215 of these residues and testing their activity in converting PR-Ub into ADPR-Ub. Mutations
216 in S261, H305 or E309 completely abolished the enzymatic activity (**Fig. 4a-b**).

217 To determine the role of LnaB during *L. pneumophila* infection, we employed mass
218 spectrometric analysis to probe PR-Ub in cells infected with relevant bacterial strains.
219 Very weak signals of PR-Ub were detected in cells infected with wild-type bacteria, but it
220 became abundant in cells infected with the Δ *LnaB* mutant. Complementation with LnaB
221 but not the LnaB_{S261A} mutant rendered PR-Ub undetectable (**Fig. 4c**), indicating that LnaB
222 functions to eliminate PR-Ub in infected cells.

223

224 We also examined the distribution of LnaB in cells infected with *L. pneumophila*
225 but were not able to detect signals using our antibodies specific for this protein. Yet,
226 results from infection of cells transfected to express 4Flag-LnaB indicated that the protein
227 was enriched on the LCV and such enrichment was dependent upon an active Dot/Icm
228 system as vacuoles containing the *dotA* mutant did not detectably recruit Flag-LnaB
229 (Supplementary **Fig. 9a**). These results suggest that similar to MavL, LnaB likely acts on
230 the surface of the bacterial phagosome.

231

232 Similar to earlier experiments, in cells infected with wild-type *L. pneumophila*,
233 ADPR-Ub is detected and adding LnaB led to a slight increase in its abundance (**Fig. 4d**).

234 Importantly, ADPR-Ub was not detectable in cells infected with the $\Delta InaB$ mutant but
235 became abundant after adding recombinant LnaB (**Fig. 4d**), which is consistent with the
236 notion that PR-Ub was accumulated in these cells. PR-Ub accumulation caused by
237 infections with strain $\Delta InaB$ can be reversed by complementation with LnaB but not the
238 LnaB_{S261A} mutant (**Fig. 4d**). LnaB-dependent elimination of PR-Ub in infected cells by
239 converting it into ADPR-Ub with recombinant LnaB was also determined. We also probed
240 the ratio of PR-Ub in cells infected with the $\Delta InaB$ mutant by mass spectrometric analysis,
241 which revealed that more than 30% of ubiquitin was modified in the PR-Ub form under
242 our experimental conditions (**Fig. 4e**). Finally, PR-Ub was not detected in cells infected
243 with the $\Delta dupA\Delta dupB$ mutant (Supplementary **Fig. 9b**), expression of either gene but not
244 their enzymatically inactive mutants in this strain restored its accumulation in infected
245 cells, indicating that PR-Ub is produced by reversal of SidEs-induced ubiquitination.
246 Together, these results establish that LnaB functions to covert PR-Ub into ADPR-Ub in
247 infected cells.

248 The conversion of PR-Ub and ADPR-Ub into native ubiquitin suggests that
249 accumulation of these ubiquitin derivatives interferes with intracellular replication of *L.*
250 *pneumophila*. We thus examined the growth of relevant *L. pneumophila* strains in
251 *Dictyostelium discoideum*. Consistent with results from an earlier study²⁷, deletion of *InaB*
252 did not detectably impact intracellular bacterial replication (**Fig. 4f**). Overexpression of
253 pSdeA in the wild-type strain led to a reduction in bacterial growth and such growth
254 defects became more pronounced when SdeA was expressed in the $\Delta InaB$ strain. In
255 contrast, expression of the mART-defective mutant SdeA_{E/A} or SdeA_{H/A}, the mutant
256 defective in the phosphodiesterase (PDE) activity in the $\Delta InaB$ mutant did not cause such
257 defect (**Fig. 4f**). Importantly, the growth defect can be complemented by expressing LnaB
258 but not its enzymatically inactive mutant (**Fig. 4f**). Taken together, these results suggest
259 that accumulation of PR-Ub in host cells is detrimental to intracellular bacterial growth
260 and the effects became more severe when the expression level of SidEs such as SdeA
261 was increased in the bacterium, and that LnaB ameliorates such impact by eliminating it
262 in infected cells.

263

264 **LnaB and tested members of the S-HxxxE family catalyze protein AMPylation**

265 Incubation of ³²P- α -ATP with LnaB in the absence of PR-Ub generated radio-labeled

266 LnaB (**Fig. 2f, 2nd lane**), suggesting that this enzyme is capable of catalyzing protein
267 AMPylation by transferring the AMP moiety from ATP onto one or more of its own residues.
268 Indeed, mass spectrometric analysis revealed that both Y196 and Y247 were AMPylated
269 (**Fig. 5a-b and Supplementary Fig. 9c-d**). Mutations in both Y196 and Y247 gave rise to
270 a mutant that had lost the ability to self-AMPylyate, but retained the activity to convert PR-
271 Ub into ADPR-Ub (**Fig. 5b-c**). These results establish LnaB as an enzyme that catalyzes
272 the cleavage of ATP at the α phosphate position to transfer the AMP moiety onto the
273 phosphoryl group in PR-Ub and the side chain of tyrosine residues.

274
275 To determine the AMPylator activity of the S-HxxxE family, we purified
276 recombinant proteins of a selection of toxins and evaluated their self-modification using
277 ^{32}P - α -ATP. For the five toxins examined, self-AMPylation was readily detected for the
278 toxin from *Burkholderia ambifaria* (Tba675) and a fragment of the toxin from *Edwardsiella*
279 *ictaluri* (Tei158) (**Fig. 5d**). Weak but detectable self-AMPylation was detected for
280 WP_075066242.1 (0750) from *Candidatus Berkiella aquae*, WP_148338824.1 (1483)
281 from *Aquicella siphonis*, MAZ44397.1 (MAZ443) from a bacterium of the Legionellales.
282 In each case, an intact S-HxxxE motif was required for the activity as mutations in the
283 serine residue abolished self-AMPylation (**Fig. 5d**). Furthermore, we found that Tei158
284 and Tba675 were toxic to yeast in a manner that requires an intact S-HxxxE motif (**Fig.**
285 **5e**). The lack of toxicity by other tested toxins suggested that their cellular targets are
286 absent in yeast or that such targets are not essential for yeast viability.

287
288 **The LnaB-Actin complex reveals an AMPylator that recognizes ATP by a unique**
289 **mechanism** To analyze the catalytic mechanism of LnaB, we solved the crystal structure
290 of the LnaB₁₉₋₃₇₁-Actin complex, which had activity indistinguishable from that of full-length
291 protein (**Fig. 6**). The asymmetric unit (ASU) of the structure contains five LnaB₁₉₋₃₇₁ and
292 six Actin molecules, which form three LnaB₁₉₋₃₇₁-Actin heterodimeric complex
293 (Supplementary **Fig. 10a**). In the LnaB₁₉₋₃₇₁-Actin complex, Actin mainly docks onto the
294 carboxyl helix α 14 of LnaB₁₉₋₃₇₁ (**Fig. 6a**) with an interface area of 1763.9 Å². The structure
295 of LnaB contains fourteen helices and a long loop that fold into two subdomains: The N-
296 terminal domain (NTD) and the catalytic domain (CD). Structural homology search of
297 LnaB₁₉₋₃₇₁ with the DaLi server did not yield any significant hits, suggesting that it is a

298 novel folding protein. Interestingly, S261, H305, and E309, the three residues critical for
299 catalysis form a continuous platform located in an area that has concentrated positive
300 electrostatic potential (**Fig. 6b**), which may be the site for protein-protein or protein-
301 substrate interactions.

302 Two regions of LnaB₁₉₋₄₄₁ are in direct contact with Actin via extensive polar and
303 hydrophobic interactions: a long loop consisting of a pair of antiparallel β -sheet proximal
304 to the S-HxxxE motif and the carboxyl end helix α 18, which we designated as Interface1
305 and Interface2, respectively. In interface 1, T225 of LnaB engages by hydrogen-bonding
306 interaction with K113 and R116 of Actin; N220 of LnaB forms hydrogen bonds with A170
307 and Y169 of Actin; T209 of LnaB contacts residues E286 of Actin via a hydrogen bond
308 (**Fig. 6c**). In interface 2, H359 engages in hydrogen-bonding interaction with T148 and
309 E167 of Actin; E370 and Q363 form hydrogen bonds with R147 of Actin (**Fig. 6d**). Other
310 hydrogen bonds include R365(L, LnaB):S348(A, Actin), E361(L):T351(A),
311 L352(L):Y169(A), D347(L):R372(A) and Q355(L):Y143(A). L362 of LnaB inserts into a
312 hydrophobic pocket composed of I345, L346 and Y134 of Actin. Substitution of T225,
313 E361 or L362 with alanine indeed reduced LnaB activity toward PR-Ub. Yet, single
314 substitution mutation in other sites involved in its interaction with Actin did not detectably
315 affect its enzymatic activity (**Fig. 6e-f**).

316 Despite extensive efforts, we were unable to obtain crystals of the LnaB-Actin
317 complex containing ATP. We thus docked the ATP molecule into LnaB by molecular
318 docking, which revealed that ATP may bind to a positively charged pocket neighboring
319 the S261-H305-E309 motif of LnaB (**Fig. 6g and Supplementary Fig. 10b**). Alanine
320 substitution in K199, Y299 or Y304 markedly reduced LnaB activity (**Fig. 6h**) and the
321 binding of these mutants to ATP became almost undetectable (**Fig. 6i and**
322 **Supplementary Fig. 11**), validating our hypothesis that this positively charged pocket is
323 involved in ATP binding.

324

325 **Discussion**

326 Three mechanisms for protein AMPylation have been described²⁸, including the
327 Cx₁₁DxD motif employed by the glutamine synthetase from *E. coli* and the multifunctional
328 *L. pneumophila* effector SidM/DrrA²⁹⁻³¹, the Fic domain exemplified by VopS of *Vibrio*
329 *parahaemolyticus*³² and the pseudokinase domain found in widely distributed proteins of

330 the selenoprotein-O protein family³³. Differing from enzymes that only target hydroxyl-
331 containing side chains of their substrate, LnaB targets the phosphate group in PR-Ub.
332 Self-AMPylation by members of the S-HxxxE family suggests that at least a fraction of
333 these enzymes AMPylate their substrate in host cells. The Fic domain has been shown
334 to use CDP-choline³⁴ and UTP³⁵ as reactants, it is possible that some S-HxxxE proteins
335 may use other nucleotides or their derivatives as substrates for protein modification.
336 AMPylation is a reversible modification, signaling by this mechanism can be modulated
337 by specific stimuli³⁶⁻³⁸. It is of great interest to identify enzymes involved in reversal of
338 AMPylation catalyzed by these diverse modifiers.

339 The requirement of a host cell-specific co-factor allows pathogens to restrict the
340 activity of virulence factors within target cells. For instance, both the edema factor of
341 *Bacillus anthracis* and CyaA of *Bordetella pertussis*^{39,40} use calmodulin (CaM) as the co-
342 factor to ensure that cAMP is generated only in host cells. The requirement of CaM by
343 the glutamylase SidJ is to prevent premature inactivation of SidEs in *L. pneumophila*^{20,21}.
344 PR-Ub has only been found in cells infected by *L. pneumophila*^{7,9,10} produced by DupA
345 and DupB from proteins modified by SidEs. Our results have highlighted the importance
346 of ubiquitin homeostasis in cells infected by *L. pneumophila* (**Fig. 7**). Yet, the reason for
347 the requirement of Actin for LnaB activity is less clear. Actin dependence may prevent
348 LnaB-induced ATP depletion or active LnaB may recognize phosphoribose-bearing
349 metabolites in bacterial cells. Alternatively, binding to Actin may facilitate the targeting of
350 host proteins of relevant cellular processes such as NFκB signaling. Further investigation
351 of the catalytic mechanism of LnaB, the function of toxins of this family, and the potential
352 use of the S-HxxxE motif by eukaryotic cells in signaling will shed insights into not only
353 protein biochemistry but also novel cell signaling cascades potentially important for
354 development and disease.

355 **Limitations of the Study** Although we have shown that LnaB and MavL function
356 sequentially to convert PR-Ub produced by reversing phosphoribosyl ubiquitination
357 induced by members of the SidE effector family, a few important questions remain. First,
358 when do the activities of LnaB and MavL become important during *L. pneumophila*
359 infection? More sensitive detection methods are needed to probe temporal translocation
360 of relevant effectors, including SidEs, DupA, DupB, MavL and LnaB and the relative
361 abundancy of these effectors needs to be correlated with the abundancy of PR-Ub and

362 ADPR-Ub in infected cells. Second, what is the level of PR-Ub or ADPR-Ub required for
363 detectable defects in intracellular bacterial growth? For the S-HxxxE toxins, future
364 investigation may focus on their cellular targets, their role in virulence. The mechanism of
365 catalysis by these proteins also awaits further study. For example, how do these toxins
366 modify their targets? Do they transfer the AMP moiety to hydroxyl groups on the side
367 chain of the target residues? or like LnaB, to a phosphate group? Finally, it will be of great
368 interest to investigate whether this motif is used for catalyzing AMPylation by proteins of
369 eukaryotes for signaling.

370

371 **Acknowledgements**

372

373 This work was supported in part by the National Natural Science Foundation of China
374 grants 32370185 (JF), 32270185 (LS), 82225028 and 82172287 (SO), 31900879 and
375 32171265 (HG), 21974002 and 22174003 (XL), the National Key Research and
376 Development Program of China 2021YFC2301403 (SO) 2022YFA1304500 (XL) and the
377 High-level personnel introduction grant of Fujian Normal University (Z0210509) (SO), and
378 by National Institutes of Health grants R01AI127465 and R01GM126296. Mass
379 spectrometric analysis was performed in the core facility of the First Hospital of Jilin
380 University, the authors thank Dr. Naicui Zhai for assistance.

381

382 Structures discussed in the paper have been deposited in Protein Data Bank
383 (<http://rcsb.org>) with the codes: 8J9B (LnaB-Actin complex), 8IPW (MavL-ADPR), and
384 8IPJ (MavL₍₄₀₋₄₀₄₎D315A-ADPR-Ub).

385

386 **Author contributions** ZQL, JF, XL, SO and LS conceived the ideas for this work. Unless
387 otherwise specified, JF, SL and CL performed the biochemical experiments and infection
388 experiments. LS performed the yeast experiments; HG and ZZ performed the
389 experiments with MavL, YL and QG performed the bioinformatics analysis, JF, WX and
390 XL performed mass spectrometric analyses. HG, TTC, JW, QL, LK, SZ and SO performed
391 structural studies and analyzed protein binding using biophysical tools. JL and SX
392 performed the molecular docking. ZQL, JF, XL, LS, SO and CD interpreted the results.
393 ZQL wrote the manuscript and all authors provided editorial input.

394

395 **Competing interests**, the authors declare no conflict of interest.

396 **Figure titles and legends**

397

398 **Fig. 1 MavL is a macro domain protein that converts ADPR-Ub into ADP-ribose and**
399 **ubiquitin**

400 **a.** Hydrolysis of ADPR-Ub into ADPR and Ub by MavL DupA or DupB. Recombinant
401 proteins were incubated with ADPR-Ub and the production of native Ub was detected by
402 native polyacrylamide gel electrophoresis (upper panel). Native Ub, PR-Ub and ADPR-
403 Ub were loaded separately as controls. Identical samples separated by SDS-PAGE were
404 detected by CBB staining, phosphoprotein stain or immunoblotting with an ADPR-specific
405 antibody (lower three panels).

406 **b.** Mutational analysis of residues important for the de-ADP ribosylation activity of MavL.
407 Recombinant MavL or its mutants were incubated with ADPR-Ub and the reduction of the
408 reactant was detected by immunoblotting with an ADPR-specific antibody.

409 **c.** Binding of Ub, ADPR-Ub and ADPR to MavL₄₀₋₄₀₄ or its mutants. Binding affinity was
410 evaluated using a low volume Nano ITC set at 20°C.

411 **d.** Ribbon diagram representation of the MavL_{(40-404)D315A}-ADPR-Ub complex. Ub, ADPR
412 and MavL are colored in pink, yellow and cyan, respectively. The recognition of ADPR-
413 Ub by MavL as well as the interactions between the two proteins are shown in the middle
414 panel. **The 2mFo-DFc(blue) and mFo-DFc (green) electron-density maps of the key**
415 **residues of MavL, Ub and water surrounding ribose involved in forming the catalytic**
416 **center are contoured at the 1.5 σ and 3.0 σ levels and shown in the right panel.** It
417 represents the transient state of the substrate catalyzed by MavL. The N-glycosidic bond
418 between the side chain of R42 in Ub and the ADPR moiety was cleaved, as indicated by
419 the red dashed lines and arrow.

420 **e.** The overall structure of MavL_{(40-404)D315A}-ADPR-Ub and its comparison to Apo MavL
421 (gray) and MavL-ADPR (blue). The conformational changes that contribute to the opening
422 of the catalytic pocket to facilitate the binding of ADPR-Ub and the subsequent reaction
423 were shown. Residues that cause steric hindrance between Apo MavL and Ub were
424 marked with red dashed circles.

425 **f.** MavL reduces the level of ADPR-Ub in infected cells. The indicated *L. pneumophila*
426 strains were used to infected cells expressing 3xHA-Ub and the accumulation of ADPR-
427 Ub was detected after HA antibody immunoprecipitation. Expression of Flag-MavL and

428 its mutant was detected with Flag antibody and isocitrate dehydrogenase (ICDH) was
429 probed as a loading control.

430

431 **Fig. 2 Conversion of PR-Ub into ADPR-Ub by LnaB requires Actin as a co-factor**

432 **a.** Native lysates of mammalian cells activate LnaB. Native (N) or boiled (B) lysates of
433 293HEK cells were added to reactions containing PR-Ub, MavK or LnaB and the
434 production of ADPR-Ub was detected by immunoblotting.

435 **b.** Identification of Actin as a LnaB-binding protein. Flag-LnaB expressed in HEK293T
436 cells was isolated by immunoprecipitation and the bound proteins were identified by mass
437 spectrometry. Similarly obtained samples with Flag-RavN were used as a control. alpha
438 Actin (ACTC1) and beta Actin-like 2 (ACTBL2) were the among the most abundant
439 proteins identified.

440 **c.** Interactions between LnaB and Actin measured by ITC. Raw ITC curves (top panel)
441 and binding isotherms with fitting curves (bottom panel) of LnaB titration by Actin. The
442 thermogram is a monophasic curve with an inflection point at molar ratio of 0.84. The
443 binding affinity is approximately 1.24 μM and the stoichiometry is 1:1 of Actin:LnaB. **The**
444 **thermodynamic parameters were also shown, ΔH : -6.88 $\text{kJ}\cdot\text{mol}^{-1}$ and ΔS : 88.75 $\text{J}\cdot\text{mol}$**
445 **$^{-1}\cdot\text{K}^{-1}$.**

446 **d.** LnaB and actin utilize ATP to convert PR-Ub into ADPR-Ub. Actin was added to a
447 subset of reactions containing LnaB and PR-Ub. Samples separated by SDS-PAGE were
448 probed for ADPR-Ub (upper panel), ubiquitin, LnaB or Actin by immunoblotting with
449 antibodies specific for each protein or its epitope tag.

450 **e-f.** LnaB transfers the AMP moiety of ATP to PR-Ub. The chemical structure of ADPR-
451 Ub with the AMP moiety added to phosphate group on PR-Ub being highlighted (dashed
452 box) (e). ^{32}P - α -ATP was added to the indicated reactions and incubated at 37°C for 1 h.
453 Samples separated by SDS-PAGE were detected by CBB staining (left) and
454 autoradiograph, respectively. Note the presence of self-modified LnaB in the reaction
455 without PR-Ub (f).

456 **g.** ATP analogs with a cleavable α phosphate support LnaB activity. Samples of reactions
457 receiving the indicated ATP analogs were resolved by SDS-PAGE, and ADPR-Ub and
458 the reactants were detected by immunoblotting by antibodies specific for ADPR, Ub, LnaB
459 or Actin. Note that ApCpp is uncleavable at the α position thus did not support the activity

460 of LnaB. In each case, similar results were obtained in at least three independent
461 experiments.

462

463 **Fig. 3 LnaB and MavL sequentially convert PR-Ub into ADPR and active ubiquitin**

464 **a-b.** Detection of LnaB-mediated conversion of PR-Ub into ADPR-Ub by mass
465 spectrometric analysis. Excised protein bands from SDS-PAGE gels corresponding to
466 PR-Ub prior to the reaction or ADPR-Ub after incubated with ATP, LnaB and Actin were
467 digested with trypsin and analyzed by mass spectrometry. A reference fragment
468 T₁₂ITLEVEPSDTIENVK₂₇ was present in both samples with similar abundance (a left
469 panel). The abundance of the fragment with PR-modified R42 was high in the PR-Ub
470 samples but became almost undetectable after reaction with LnaB, ATP and Actin, which
471 was accompanied by the increase of ADPR-modified fragment. A MS/MS spectrum
472 indicating ADPR modification of R42 was shown in b.

473 **c.** A reaction scheme depicting the conversion of PR-Ub into ubiquitin by LnaB and MavL.
474 The AMPylation activity of LnaB first converts PR-Ub into ADPR-Ub, which is further
475 reduced into ADP-ribose and ubiquitin by MavL. The AMP moiety defined by a dash line
476 rectangle indicates the chemical group added to PR-Ub by LnaB.

477 **d.** The use of ADPR-Ub produced from PR-Ub by LnaB in protein modification by the
478 phosphodiesterase (PDE) activity of SdeA. PR-Ub was incubated in the indicated
479 reactions and the ability to ubiquitinate Rab33b was detected by the formation of higher
480 MW species detected by immunoblotting with the Flag-specific antibody. Native ADPR-
481 Ub was included as a control (1st lane).

482 **e.** Conventional ubiquitination by ubiquitin produced by MavL and LnaB from PR-Ub. A
483 series of reactions containing PR-Ub and combinations of relevant proteins were allowed
484 to proceed for 1 h at 37°C. The products were boiled for 5 min at 95°C and a cocktail
485 containing E1, E2, SidC (E3) and ATP was added, self-ubiquitination of SidC was
486 detected by immunoblotting with a ubiquitin-specific antibody.

487

488 **Fig. 4 The reaction catalyzed by LnaB required an S-HxxxE motif**

489 **a-b.** Conversion of PR-Ub into ADPR-Ub by LnaB requires an S-HxxxE motif. Samples
490 of reactions containing ATP, PR-Ub, LnaB, Actin, LnaB or its mutants and resolved by
491 SDS-PAGE were detected for the production of ADPR-Ub (top). Each reactant was

492 detected by immunoblotting with the appropriate antibodies (a). Similar reactions with ^{32}P -
493 α -ATP were established, proteins were detected by CBB staining (upper) and the
494 production of ^{32}P -ADPR-Ub was detected by autoradiograph (lower) (b).

495 **c-d.** LnaB functions to convert PR-Ub into ADPR-Ub in cells infected with *L. pneumophila*.
496 HEK293 cells transfected to express 3xHA-Ub were infected with the indicated bacterial
497 strains (I to V). Immunoprecipitation products obtained by HA antibody from lysates of
498 infected cells were analyzed by mass spectrometry to detect differently modified ubiquitin
499 (c). Recombinant LnaB was added to a subset of similar prepared lysates of infected cells
500 and the accumulation of PR-Ub was assessed by detecting LnaB-mediated ADPR-Ub
501 production (d).

502 **e.** The ratio of modified ubiquitin (PR-Ub) in cells infected with the Δ *InaB* mutant. Cells
503 expressing HA-ubiquitin was infected with strain Lp02 Δ *InaB* for 2 h. HA-ubiquitin isolated
504 by immunoprecipitation was analyzed by mass spectrometry to determine the ratio of
505 modified ubiquitin.

506 **f.** Overexpression of SdeA in the Δ *InaB* mutant affects intracellular bacterial growth *D.*
507 *discoideum* was infected with the indicated *L. pneumophila* strains and the growth of the
508 bacteria was evaluated. Note that strain Δ *InaB*(pSdeA) displayed significant defects in
509 intracellular growth (upper panel). The expression of SdeA in the testing strains was
510 probed by immunoblotting (lower panel). Data shown were one representative of three
511 independent experiments done in triplicate with similar results.

512

513 **Fig. 5 Self-AMPylation activity of members of the S-HxxxE toxin family**

514 **a.** LnaB self-AMPylates at Y196 and Y247. Protein bands corresponding to LnaB from
515 the indicated reactions were analyzed to identify the modified residues by mass
516 spectrometry.

517 **b-c.** Mutations of the AMPylated Tyr residues abolished the activity of LnaB. LnaB or its
518 mutants was incubated with ^{32}P - α -ATP and Actin and production of self-modified protein
519 was detected by autoradiograph (b). Similar reactions receiving PR-Ub were established
520 to probe the impact of the mutations on the conversion of PR-Ub into ADPR-Ub, which
521 was detected by immunoblotting (top) and the proteins in the reactions were detected by
522 CBB staining (lower).

523 **d.** Self-AMPylation by members of the S-HxxxE family. Recombinant proteins of the
524 indicated toxins were incubated with ^{32}P - α -ATP and Actin. Samples resolved by SDS-
525 PAGE were detected for AMPylation by autoradiograph (lower) and for the proteins by
526 CBB staining (upper). Red arrows indicated AMPylated proteins. Note that in each case,
527 self-AMPylation required an intact S-HxxxE motif.

528 **e.** Yeast toxicity by the toxins required an intact S-HxxxE motif. Serially diluted cells of
529 yeast strains expressing the indicated toxin genes or their S-HxxxE mutants were spotted
530 on medium containing glucose or galactose. Images were acquired after 3-day incubation
531 at 30°C (left). The expression of the proteins was probed by immunoblotting with the Flag-
532 specific antibody. The phosphoglycerate kinase (PGK) was probed as a loading control.

533

534 **Fig. 6 LnaB-Actin binary complex structure reveals a unique catalytic mechanism**
535 **on AMPylation**

536 **a.** Cylindrical cartoon diagram representation of the LnaB-Actin complex. The top panels
537 represent schematic diagrams of the regions for domain organization of LnaB and Actin.
538 LnaB consists of the N-terminal domain (NTD, purple), the catalytic domain (CD, orange)
539 and the C-terminal domain (CTD, grey); Actin is composed of NTD (green) and CTD
540 (Limon). S261, H305 and E309 of the S-HxxxE motif are shown in red. The bottom panel
541 shows the LnaB-Actin binary structure. Domains of LnaB and Actin were colored in
542 accordance with the diagrams (top). The interfaces involved in LnaB-Actin interactions
543 were highlighted in two dashed line circles.

544 **b.** S261, H305 and E309 formed a platform in the structure of LnaB. Residues were
545 represented as sticks and LnaB was depicted in surface, colored according to the
546 electrostatic surface potential [contoured from -6kBT (red) to +6kBT (blue)].

547 **c-d.** The interfaces involved in LnaB-Actin interactions. LnaB and Actin were shown as
548 orange and green cartoons, respectively. Residues important for binding were shown as
549 sticks (Actin in green and LnaB in orange). Hydrogen bonds were marked by blue dashed
550 lines.

551 **e.** Optimal binding to Actin is required for maximal activity of LnaB. Indicated LnaB
552 mutants were individually incubated with Actin, ATP, and PR-Ub for 30 min at 37°C and
553 their activity in converting PR-Ub into ADPR-Ub was evaluated by immunoblotting with
554 an ADPR-specific antibody. Proteins in the reactions were detected by CBB staining.

555 **f.** Evaluation of the binding of Actin to LnaB and its mutants by Ni²⁺ beads pulldown. His₆-
556 LnaB and its mutants were individually incubated with Actin at 4°C for 6 h prior to pulldown
557 with Ni²⁺ beads. Actin was detected using anti-Actin antibodies and proteins were
558 detected by CBB staining.

559 **g-i.** An ATP-binding pocket in LnaB identified by molecular docking. LnaB was displayed
560 in a grey surface model. Residues potentially involved in binding ATP was indicated as
561 orange sticks. ATP was shown as a cyan stick-ball model and hydrogen bonds were
562 represented by blue dashed lines (G). LnaB mutants were evaluated for the ability to
563 convert PR-Ub into ADPR-Ub with reactions described above. Proteins were detected by
564 CBB staining (H). The affinity between ATP and LnaB and its mutants was determined
565 using isothermal titration calorimetry (ITC). The binding constant (K_d) was calculated by
566 the NanoAnalyze software package. Data shown are one representative of three
567 independent experiments with similar results (E, F, H and I).

568

569 **Fig. 7** The cycling of ubiquitin by Dot/Icm effectors in cells infected by *L. pneumophila*.
570 Ubiquitin is converted into ADPR-Ub by the mART activity of SidEs, which is used to
571 modified proteins by phosphoribosyl ubiquitination. The reversal of the modification
572 produced PR-Ub, which is converted into native ubiquitin by sequential reactions
573 catalyzed by LnaB and MavL. Note that both ADPR-Ub and PR-Ub may interfere with
574 canonical ubiquitin signaling and that ADPR-Ub produced from PR-Ub by LnaB may be
575 used by the PDE activity of SidEs for protein modification.

576

577 **Methods**

578 **Media, bacteria strains, plasmid construction and cell lines**

579 *Escherichia coli* strains were grown on LB agar plates or in LB broth. When
580 necessary, antibiotics were added to media at the following concentrations: ampicillin,
581 100 µg/mL; kanamycin, 30 µg/mL. *L. pneumophila* strains used in this study were
582 derivatives of the Philadelphia 1 strain Lp02⁴¹. Lp03 is an isogenic *dotA*⁻ mutant⁴¹. All
583 strains were grown and maintained on CYE plates or in ACES-buffered yeast extract
584 (AYE) broth as previously described⁴¹. When needed, thymidine was added at a final
585 concentration of 100 µg/mL. The Lp02Δ*dupA*Δ*dupB* mutant was described earlier⁹.
586 Mutants lacking *mavL* or *InaB* were constructed using strain Lp02 as previously described
587⁴². Complementation plasmids were constructed by inserting the gene of interest into
588 pZL507⁴³. The plasmid for expression SdeA, mutants SdeA_{E/A} and SdeA_{H/A} were from
589 previous studies^{6,20}. For ectopic expression of proteins in mammalian cells, genes were
590 inserted into pEGFPC1 (Clontech) or p4xFlagCMV⁶. The plasmid for expressing 3xHA-
591 Ub in mammalian cells had been described earlier⁶. Genes for purifications were cloned
592 into pGEX-6P-1 (Amersham), pQE30 (QIAGEN), pET-28a (Novagen) or pET28a-Sumo
593 (Novagen). The integrity of all constructs was verified by sequencing analysis. Genes
594 coding for WP_015869719.1 from *Edwardsiella ictaluri*, WP_006755655.1 from
595 *Burkholderia ambifaria* and WP_075066242.1 from *Candidatus Berkiella aquae*,
596 WP_148338824.1 from *Aquicella siphonis*, MAZ44397.1 from a species of Legionellales
597 were synthesized by GenScript Biotech Corp (Nanjing, China) with codon optimized for
598 *E. coli*. HEK293T cells purchased from the ATCC were cultured in Dulbecco's modified
599 minimal Eagle's medium (DMEM) supplemented with 10% Fetal Bovine Serum (FBS). All
600 mammalian cell lines were regularly checked for potential mycoplasma contamination by
601 the universal mycoplasma detection kit from ATCC (Cat# 30-1012K).

602 **Yeast toxicity assays**

603 Yeast strains were grown in YPD (1 % yeast extract, 2 % peptone, 2 % glucose) or
604 SD minimal media containing nitrogen base, glucose and amino acid drop-out mix for
605 selection of transformed plasmids as described⁴⁴. The genes coding for the testing toxins
606 was individually inserted into pYES2/NTA (Invitrogen) that carries a galactose-inducible
607 promoter⁴⁵. In each case, the sequence coding for the Flag tag was added to the amino

608 terminal end of the gene to facilitate detection of gene expression. The resulting plasmids
609 were introduced into yeast strain W303⁴⁶, respectively. Ten microliters of 5-fold dilutions
610 of saturated cultures were spotted onto dropout medium containing glucose or galactose.
611 Plates were incubated in 30°C for 3 d prior to image acquisition to assess growth. To
612 detect protein expression, cells cultured in medium containing 2% raffinose were washed
613 once with galactose medium and were induced in 2% galactose medium for 2 d at 30°C.
614

615 **Transfection, infection and immunoprecipitation**

616 Plasmids were transfected into mammalian cells by using Lipofectamine 3000
617 (Invitrogen, cat# L3000150). After 24 h transfection, cells were collected and lysed with
618 the TBS buffer (150 mM NaCl, 50 mM Tris-HCl, pH 7.5) with 1% Triton X-100. When
619 needed, immunoprecipitation was performed with lysates of transfected cells by Flag-
620 specific antibody coated agarose beads (Sigma, cat# F2426) or GFP-specific antibody
621 which was coupled to protein G beads (Cytiva, cat# 17061801) at 4°C for 8 h. Beads were
622 washed 3x with pre-cold lysis buffer. After that, Flag peptide solution (150 µg/mL) (Sigma,
623 cat# F3290) or 0.1 M glycine buffer (pH 2.5) was used to elute Flag-tagged proteins or
624 GFP-tagged proteins, respectively. All samples were resolved by SDS-PAGE and
625 followed by immunoblotting analysis with the specific antibodies.

626 For intracellular bacterial growth, *L. pneumophila* strains grown to early post
627 exponential phase ($OD_{600}=3.3-3.8$) were used to infect bone marrow-derived
628 macrophages or *D. discoideum* at an MOI of 0.05 as described earlier⁴². 2 h after adding
629 the bacteria, infections were synchronized by washing cells with warm PBS to remove
630 the extracellular bacteria and IPTG was added at a final concentration of 0.05 mM to
631 induce the expression of SdeA and its mutant. Infected cells were lysed with 0.02%
632 saponin at the indicated time points and the total viable bacterial cells were determined
633 by plating appropriate dilutions on CYE plates.

634 To determine ADPR-Ub levels in infected cells, HEK293T cells were co-
635 transfected with plasmids expressing the FcγII receptor and 3xHA-Ub⁶. The indicated *L.*
636 *pneumophila* strains were grown to the post-exponential growth phase ($OD_{600}=3.4-3.8$)
637 in AYET broth containing Kanamycin (20 µg/mL). Four h prior to infection, IPTG was
638 added into the broth at a final concentration of 0.2 mM. *L. pneumophila* cells were
639 opsonized by mixing with *L. pneumophila*-specific rabbit antibodies at a 1:500 ratio for 30

640 min at 37°C. Thirty-six h post transfection, opsonized bacteria were used to infect
641 transfected cells at an MOI of 50. 2 h post infection, cells were washed with cold PBS and
642 lysed with TBS buffer containing 150 mM NaCl, 50 mM Tris-HCl, 1 mM DTT, 1% Triton
643 X-100, following with 10% sonication for 10 s. Lysates were centrifuged twice at 20,000g
644 for 15 min and the supernatants were collected and incubated anti-HA beads at 4°C for
645 8 h. Beads were washed three times with cold lysis buffer and were boiled in 1x sample
646 buffer for 10 min.

647 To detect PR-Ub in cells infected with *L. pneumophila* strains, cell lysates obtained
648 using an infection procedure described above were divided into two identical samples,
649 and 10 µg His₆-LnaB was added to one sample and 10 µL TBS buffer was added to
650 another sample as controls. The reactions were allowed to proceed for 2 h at 37°C and
651 samples were then incubated with anti-HA beads to immunoprecipitated 3xHA-Ub by
652 incubation at 4°C for 8 h. Beads were washed three times in cold lysis buffer and were
653 boiled in 1x sample buffer for 10 min prior to SDS-PAGE.

654
655 To determine the association of MavL and LnaB with the LCV, HEK293 cells
656 transfected to express HA-MavL or 4Flag-LnaB were infected with the relevant *L.*
657 *pneumophila* strains for 1 h and the samples were stained with the appropriate antibodies.
658 The intracellular and total bacterial were distinguished by sequential immunostaining.
659 Samples were inspected and analyzed using an Olympus IX-83 fluorescence microscope.

660

661 **Protein purification**

662 For His₆- or GST-tagged recombinant protein production for *in vitro* assays, 20 mL
663 saturated *E. coli* cultures were transferred to 400 mL LB medium supplemented with 30
664 µg/mL kanamycin or 100 µg/mL ampicillin, the cultures were grown to OD_{600nm} of 0.6-0.8
665 at 37°C. Protein expression was induced with 0.2 mM IPTG at 18°C for 16-18 h on a
666 shaker (200 rpm). Bacterial cells were collected by centrifugation and lysed by sonication.
667 The soluble lysates were cleared by spinning at 15,000g at 4°C for 30 min. Supernatant
668 containing recombinant proteins were purified by Ni²⁺-NTA beads (QIAGEN) or
669 Glutathione agarose beads (Pierce), and were eluted from beads by using PBS buffer
670 containing 300 mM imidazole or 10 mM reduced glutathione in a Tris buffer (50 mM Tris-

671 HCl, pH 8.0). Purified proteins were dialyzed against PBS buffer containing 10% glycerol
672 and 1 mM DTT at 4°C for 8 h.

673 To purify proteins for structural study, the coding regions or the truncation mutants
674 of MavL or LnaB were inserted into pET28a-sumo and the resulting plasmids each was
675 transformed into *E. coli* strain BL21(DE3). The bacterial strains were cultured at 37°C in
676 LB broth on a shaker (220 rpm) and then induced with 0.5 mM IPTG when the bacteria
677 grew to a density OD600 = 0.8. The bacteria were then cultured for 16 h at 18°C before
678 collecting the cells by centrifugation (5,000g, 15 min). Cells resuspended in a cold lysis
679 buffer (50 mM Tris-HCl pH 7.5, 150 mM NaCl) were lysed by ultrasonication. Lysates
680 were centrifuged at 35,000g for 30 min at 4°C to obtain supernatant, which was used to
681 purify His₆-tagged proteins by affinity chromatography (Ni²⁺ resin). The SUMO tag was
682 removed by the SUMO protease ULP1. Proteins were further purified by size-exclusion
683 chromatography using a Superdex 200 Increase column (GE Healthcare) equilibrated
684 with a buffer containing 25 mM HEPES, pH 7.5, 150 mM NaCl, and 2 mM DTT. The best
685 fractions of protein peak were pooled, concentrated to 10 mg/mL with an Amicon
686 Centrifugal filter (Millipore), flash-frozen in liquid nitrogen and stored at -80°C for
687 crystallization and activity assay. Protein concentration was measured at A280 and
688 calculated using their theoretical extinction coefficients.

689

690 **Isothermal titration calorimetry**

691 Isothermal titration calorimetry ITC experiments were carried out using a Low
692 Volume Nano ITC (TA instruments) set at 20°C. Protein of MavL or its mutants and ADPR
693 were dissolved in the buffer containing 50 mM Tris-HCl, pH 7.5, and 150 mM NaCl. The
694 concentration of ADPR in the syringe was 1 mM and the concentrations of proteins in the
695 sample cell were 0.1 mM. Twenty-five consecutive 2 µl injections of ADPR were titrated
696 into a 350 µl sample cell with a 200 s interval between injections using a stirring rate of
697 120 rpm. A single - site binding model was used for nonlinear curve fitting using the
698 Launch NanoAnalyze software provided by the manufacturer.

699 LnaB-Actin binding was performed using a microcalorimeter Affinity ITC (Waters™,
700 USA) at 20°C. LnaB and its mutants purified as above was diluted into a buffer of 50 mM
701 Tris-HCl and 150 mM NaCl to a final concentration of 0.2 mM. Actin (Sangon Biotech,
702 A001041) was prepared in the same buffer at concentration of 22 µM. To measure LanB-

703 ATP binding, Concentrations of LnaB or its mutants and ATP were 0.1 mM and 1 mM,
704 respectively. Titrations were set for 20 injections and each of 2 μ L with 200 s intervals
705 except from the first injection of 0.2 μ L. Baseline subtraction and data analysis were
706 performed using NanoAnalyze (WatersTM, USA). Heat spikes were integrated and fitted
707 with 1:1 binding model. The first injection was excluded from analysis.

708

709 **Analytical ultracentrifugation (AUC)**

710 Sedimentation velocity (SV) experiments were performed in buffer containing 50 mM Tris-
711 HCl, pH 8.0 and 150 mM NaCl using Proteomelab XL-I Analytical Ultracentrifuge
712 (Beckman-Coulter). In AUC-SV analysis, runs were carried out at 50,000 r.p.m. and at a
713 temperature of 10.0 °C using 12 mm charcoal-epon double sector centerpieces and An60
714 Ti analytical rotor. The evolution of the resulting concentration gradient was monitored
715 with absorbance detection optics at 280 nm, All AUC-SV raw data were analysed by the
716 continuous C(s) distribution model implemented in the programme SEDFIT⁴⁷. Partial
717 specific volume and extinction coefficient of the protein as well as buffer density and
718 viscosity, were calculated from amino acid and buffer composition, respectively, by the
719 program SEDNTERP⁴⁸ and were used to calculate protein concentration and correct
720 experimental s-values to $s_{20,w}$.

721

722 **Ni²⁺-agarose affinity pull-down assays**

723 This assay was carried out in the binding buffer 150 mM NaCl, 20 mM Tris pH 8.0,
724 20 mM imidazole, and 0.02% Triton X-100. 1 mL of reaction mixture including 70 μ g His-
725 tagged LnaB or its mutants, and 20 μ g Actin, was incubated at 4 °C. After 4 h, 20 μ L of
726 nickel sepharose beads were added and incubated for another 1 h. The bound beads
727 were added with 1.25 \times SDS-loading buffer and boiled at 95°C for 10 min after washing
728 three times with the binding buffer, then separating by SDS-PAGE and detecting by an
729 anti-Actin antibody.

730 **Biochemical AMPylation assays**

731 In a 20 μ L reaction, 1 μ g His₆-LnaB or its mutants, 1 μ g Actin (Cytoskeleton, cat#
732 APHL99) and 1.5 μ g PR-Ub were used in a solution containing 50 mM Tris-HCl (pH 7.5),
733 5 mM MgCl₂ and 1 mM ATP, and the reaction was allowed to proceed for 1 h at 37°C. To

734 measure the activity of LnaB using ATP- α -³²P, 1 μ g His₆-LnaB, 1 μ g Actin (Cytoskeleton,
735 cat# APHL99) and 1.5 μ g PR-Ub were incubated in a 20 μ L reaction system containing
736 50 mM Tris-HCl (pH 7.5), 5 mM MgCl₂ and 5 μ Ci ATP- α -³²P (Perkin Elmer, cat#
737 BLU003H250UC) for 1 h at 37°C. Samples were resolved by SDS-PAGE and gels were
738 stained with Coomassie brilliant blue. Gels were then dried and the signals were detected
739 with x-ray films.

740 For the AMPylation activity of the selected members of the S-HxxxE family proteins,
741 1 μ g His₆-LnaB or homologous proteins and 0.5 μ g actin were incubated in a 20 μ L
742 reaction system containing 50 mM Tris-HCl (pH 7.5), 5 mM MgCl₂ and 5 μ Ci ATP- α -³²P
743 for 2 h at 37 °C. Products were resolved by 12% SDS-PAGE at 100V for 2 hr. Gels were
744 stained with Coomassie brilliant blue (CBB) for 1 h, de-stained twice for 2 h and then dried
745 for 8 h. Signals were detected with X-ray films using a BioMax TranScreen LE (Kodak)
746 for 4 h at RT.

747 **Biochemical de-ADP-ribosylation assays**

748 To examine the activity of MavL on different modified ubiquitin, 2 μ M MavL was
749 incubated with 100 μ M ADPR-Ub, PR-Ub or Ub for 30 min at 37°C in a solution containing
750 50 mM Tris-HCl (pH 7.5). Proteins in reactions resolved by native PAGE or SDS-PAGE,
751 were detected by Coomassie blue stain or by immunoblotting with the anti-ADPR antibody.
752 To determine the activity of MavL, DupA and DupB against ADPR-Ub, 2 μ M MavL, DupA
753 or DupB was incubated with 100 μ M ADPR-Ub for 30 min at 37°C in a solution containing
754 50 mM Tris-HCl (pH 7.5). Samples resolved by native PAGE or SDS-PAGE were detected
755 by Coomassie blue stain, phosphoprotein stain (ABP Biosciences) or immunoblotting with
756 the anti-ADPR antibody.

757 To examine the specificity of de-ADP-ribosylation activity of MavL, we prepared
758 several ADP-ribosylated proteins including ADPR-Actin catalyzed by SpvB of *Salmonella*
759 *enterica*¹⁴, ADPR-ANT1 by Ceg3 of *L. pneumophila*¹⁵, ADPR-PARP1 by Sirt6¹⁶. In each
760 case the substrate protein and the enzyme were co-expressed in 293HEK cells by
761 transfection and the ADP-ribosylated proteins were isolated by immunoprecipitation using
762 beads coated with antibody specific for the Flag or HA tag. ADPR-T66-Ub was generated
763 by incubating His₆-ubiquitin with GST-CteC of *C. violaceum*¹³. Each of the ADP-
764 ribosylated proteins was incubated with MavL or MavL_{D323A} for 30 min at 37°C and de-
765 ADP-ribosylation effects were probed by immunoblotting using the anti-ADPR antibody.

766 **Biochemical ubiquitination assays**

767 For SdeA-mediated ubiquitination reaction, 2 µg His₆-LnaB, 1.5 µg Actin
768 (Cytoskeleton, cat# APHL99) and 6 µg PR-Ub were preincubated in a 25 µL reaction
769 system containing 50 mM Tris-HCl (pH 7.5), 5 mM MgCl₂ and 1 mM ATP for 1 h at 37°C.
770 After preincubation, a cocktail containing 0.1 µg His₆-SdeA_{E/A} and 0.6 µg His₆-4xFlag-
771 Rab33b were supplemented into reactions and the reaction was allowed to proceed for
772 another 2 h at 37°C.

773 For SidC-mediated ubiquitination reaction ⁴⁹, 0.3 µg GST-E1, 1 µg His₆-UbcH7, 3
774 µg GST-SidC₁₋₅₄₂ and 4 µg Ub were incubated in a 20 µL reaction system containing 50
775 mM Tris-HCl (pH 7.5), 5 mM MgCl₂, 1 mM DTT and 2 mM ATP for 1 h at 37°C.

776 To test the ability of LnaB and MavL to convert PR-Ub into active ubiquitin, 1.5 µg
777 His₆-LnaB, 1.5 µg Actin, 1.5 µg GST-MavL and 4 µg PR-Ub were preincubated in a 25 µL
778 reaction system containing 50 mM Tris-HCl (pH 7.5), 5 mM MgCl₂ and 1 mM ATP for 1 h
779 at 37°C. After preincubation, reactions were boiled for 5 min at 95°C, then a cocktail
780 containing 0.3 µg GST-E1, 1 µg His₆-UbcH7, 3 µg GST-SidC₁₋₅₄₂, 1 mM DTT and 2 mM
781 ATP were supplemented into these boiled reactions and the reaction was allowed to
782 proceed for another 1 h at 37°C.

783

784 **Antibodies and Immunoblotting**

785 Purified His₆-GFP and His₆-GST proteins were used to raise rabbit specific
786 antibodies using a standard protocol (Pocono Rabbit Farm & Laboratory). These
787 antibodies were affinity purified as described. Antibodies specific for SdeA had been
788 described ⁶. For immunoblotting, samples resolved by SDS-PAGE were transferred onto
789 0.2 µm nitrocellulose membranes (Bio-Rad, cat# 1620112), which were blocked with 5%
790 non-fat milk or 3% BSA at R.T. for 1 h prior to being incubated with the appropriate primary
791 antibodies: anti-Flag (Sigma, cat# F1804), 1:5000; anti-Actin (MP Biochemicals, cat#
792 0869100), 1:5000; anti-tubulin (DSHB, E7) 1:10,000; anti-ADPR (Sigma, cat#
793 MABE1016), 1:1000, anti-His (Sigma, cat# H1029), 1:5000; anti-Ub (Santa Cruz, P4D1,
794 cat# sc-8017), 1:1000. Membranes were then incubated with appropriate IRDye infrared
795 secondary antibodies and scanned by an Odyssey infrared imaging system (Li-Cor's
796 Biosciences).

797

798 **LC-MS/MS analysis**

799 Protein bands were digested in-gel with trypsin as previously described⁵⁰.
800 Digested peptides were analyzed by LC-ESI-MS/MS using the Dionex UltiMate 3000
801 RSLC nano System coupled to the Q Exactive™ HF Hybrid Quadrupole-Orbitrap Mass
802 Spectrometer (Thermo Scientific, Waltham, MA). The reverse phase peptide separation
803 was accomplished using a trap column (300 µm ID × 5 mm) packed with 5 µm 100 Å
804 PepMap C18 medium, and then separated on a reverse phase column (50 cm
805 long × 75 µm ID) packed with 2 µm 100 Å PepMap C18 silica (Thermo Fisher Scientific,
806 Waltham, MA). The column temperature was maintained at 50°C.

807 Mobile phase solvent A was 0.1% FA in water and solvent B was 0.1% FA in 80%
808 ACN. Loading buffer was 98% water/2% ACN/0.1% FA. Peptides were separated by
809 loading into the trap column in a loading buffer for 5 min at 5 µL/min flow rate and eluted
810 from the analytical column at a flow rate of 150 nL/min using a 130 min LC gradient as
811 follows: linear gradient of 5% to 27% of solvent B in 80 min, 27-45% in next 20 min, 45-
812 100% of B in next 5 min at which point the gradient was held at 100% of B for 7 min before
813 reverting back to 2% of B at 112 min, and held at 2% of B for next 18 min for equilibration.
814 The mass spectrometer was operated in positive ion and standard data-dependent
815 acquisition mode with Advanced Peak Detection function activated for the top 20n. The
816 fragmentation of precursor ion was accomplished by stepped normalized collision energy
817 setting of 27%. The resolution of Orbitrap mass analyzer was set to 120,000 and 15,000
818 for MS1 and MS2, respectively. The full scan MS1 spectra were collected in the mass
819 range of 350-1,600 *m/z*, with an isolation window of 1.2 *m/z* and a fixed first mass of 100
820 *m/z* for MS2. The spray voltage was set at 2 and Automatic Gain Control (AGC) target of
821 4e5 for MS1 and 5e4 for MS2, respectively.

822 For protein identification, the raw data were processed with the software MaxQuant
823 (version 1.6.3.3) against *Homo sapiens* database (Uniprot, UP000005640) or *L.*
824 *pneumophila* database (Uniprot, UP000000609). MaxQuant was set to search with the
825 following parameters: peptide tolerance at 10 ppm, MS/MS tolerance at 0.02 Da,
826 carbamidomethyl (C) as a fixed modification, oxidation (M) as a variable modification, and
827 maximum of two missed cleavages. The false-discovery rates (FDR) were controlled at
828 <1%. To identify the Phosphoribosylation or ADP-ribosylation modification peptides, raw
829 data were analyzed manually in Xcalibur QualBrowser.

830

831 **Crystallization, data collection, and structural determination**

832 Crystallization of the complexes of MavL-ADPR, MavL_{40-404(D315A)}-ADPR-Ub and
833 LnaB-Actin were conducted using the hanging-drop vapor diffusion method at 16°C, with
834 drops containing 0.5 µl of the protein solution mixed with 0.5 µl of reservoir solution.
835 Diffraction quality of the MavL-ADPR complex crystals was obtained in 0.25M potassium
836 citrate tribasic monohydrate, 18% PEG3350, and MavL_{40-404(D315A)}-ADPR-Ub complex
837 crystals was obtained in 0.1 M HEPES/sodium hydroxide pH7.5, 20% polyethylene glycol
838 10,000, respectively. LnaB-Actin complex crystals were observed in 0.15 M Ammonium
839 sulfate, 0.1 M Sodium HEPES pH 7.0, 20% (w/v) polyethylene glycol (PEG) 4,000 after
840 one week. After optimization, the best crystals of LnaB-Actin were obtained in 0.15 M
841 Ammonium sulfate, 0.1 M Sodium HEPES pH 7.0, 22% (w/v) PEG 4,000. Crystals were
842 harvested and flash-frozen in liquid nitrogen with 20% glycerol as a cryoprotectant.
843 Complete X-ray diffraction data sets were collected at the BL02U1 beamline of the
844 Shanghai Synchrotron Radiation Facility (SSRF). Diffraction images were processed with
845 the HKL-2000 program. Molecular Replacement was then performed with the model of
846 Apo MavL (PDB:6OMI) and Ub (PDB:6K11) as a template to determine the structure of
847 the MavL-ADPR (PDB:8IPW) and MavL_{40-404(D315A)}-ADPR-Ub (PDB:8IPJ) complexes,
848 respectively. The Actin and LnaB structures (1-361 region) predicted with AlphaFold2⁵¹
849 were employed as a template. Model building and crystallographic refinement were
850 carried out in Coot and PHENIX⁵². Detailed data collection and refinement statistics are
851 listed in Table S1. The interactions were analyzed with PyMOL (<http://www.pymol.org/>)
852 and PDBsum and figures were generated with PyMOL.

853

854 **Bioinformatic identification of members of the S-HxxxE family**

855 To obtain LnaB orthologous sequences from other genera (we excluded the *Legionella*
856 genus from the blast search), we utilized PSI-BLAST²⁵ (Position-Specific Iterative Basic
857 Local Alignment Search Tool) searches at the NCBI (National Center for Biotechnology
858 Information; <http://blast.ncbi.nlm.nih.gov/>) against the nr (non-redundant) protein
859 database. We limited the PSI-BLAST search to three rounds to minimize the effect of
860 possible convergent evolution while still able to detect all the genera that contain LnaB
861 orthologs. For the purpose of phylogenetic analysis and tree construction, we first

862 removed duplicate sequences from the same species and selected closely related protein
863 sequences for analysis. Sequence alignment was generated by MAFFT⁵³ and the
864 resulting alignment was used to infer a phylogenetic tree using IQ-TREE⁵⁴. VT+F+R4
865 model was selected by the ModelFinder⁵⁵ with 1000 nonparametric replicated bootstrap
866 analysis. The obtained phylogenetic tree was visualized with iTOL web-server⁵⁶.

867

868 **Molecular docking**

869 The configuration of ATP was optimized at the B3LYP/6-31G* level using the Gaussian
870 09 package⁵⁷. The structure of LnaB was extracted from the crystal structure of the
871 LnaB/Actin complex resolved in this work. We carried out 300 independent docking runs
872 with the AutoDock 4.2 program⁵⁸ using the Lamarckian genetic algorithm (LGA)⁵⁹ as a
873 searching engine. The size of the grid box was 90×90×90 with a grid spacing of 0.375 Å.
874 The grid center was set at the center of mass of LnaB. ATP was treated as a flexible
875 molecule whereas LnaB was rigid. The results of 300 docking runs were grouped into
876 clusters according to the ligand binding conformation with default parameters
877 implemented in AutoDockTools 1.5⁵⁸. Among these cluster, there was one dominant
878 cluster accounting for 68.7% of total docking conformations (Fig. S10b). Furthermore, this
879 cluster held the lowest mean binding energy (-6.53 ± 0.41 kcal/mol) as calculated by
880 AutoDockTools 1.5 (Fig. S10b), indicating a robust structural stability. Thus, the
881 conformation with the lowest binding energy from this cluster was selected as the putative
882 complex model. The residues in the ATP binding site were defined by an atomic distance-
883 based cutoff: the residues contained at least one atom within 4.5 Å of any atom in the
884 bound ATP. Accordingly, the binding site residues of ATP included residues Y196, K199,
885 R201, P235, I237, A258-G262 and G303-H305.

886

887 **Data quantitation and statistical analyses**

888 Student's *t*-test was used to compare the mean levels between two groups each with at
889 least three independent samples. All western blot results shown are one representative
890 from three independent experiments.

891 **Data Availability**

892 Structure factors and atomic coordinates has been deposited in the Protein Data Bank
893 (PDB) under accessions: MavL-ADPR (PDB:8IPW), MavL40-404(D315A)-ADPR-Ub
894 (PDB:8IPJ), LnaB-actin (PDB:8J9B). The data that support the conclusions of this study
895 are included in this published article along with its Supplementary Information files, and
896 are also available from the corresponding author upon request. Other data, including full
897 gels, blots and LnaB interacting protein identified by IP-MS are provided in the Source
898 Data file. Source data are provided with this paper.

899

900

901 References

902

- 903 1 Lopes Fischer, N., Naseer, N., Shin, S. & Brodsky, I. E. Effector-triggered immunity
904 and pathogen sensing in metazoans. *Nat Microbiol* **5**, 14-26, doi:10.1038/s41564-
905 019-0623-2 (2020).
- 906 2 Cotter, P. A. & DiRita, V. J. Bacterial virulence gene regulation: an evolutionary
907 perspective. *Annu Rev Microbiol* **54**, 519-565,
908 doi:10.1146/annurev.micro.54.1.519 (2000).
- 909 3 Escoll, P., Mondino, S., Rolando, M. & Buchrieser, C. Targeting of host organelles
910 by pathogenic bacteria: a sophisticated subversion strategy. *Nat Rev Microbiol* **14**,
911 5-19, doi:10.1038/nrmicro.2015.1 (2016).
- 912 4 Li, Z. *et al.* Shigella evades pyroptosis by arginine ADP-ribosylation of caspase-
913 11. *Nature* **599**, 290-295, doi:10.1038/s41586-021-04020-1 (2021).
- 914 5 Qiu, J. & Luo, Z. Q. Legionella and Coxiella effectors: strength in diversity and
915 activity. *Nat Rev Microbiol* **15**, 591-605, doi:10.1038/nrmicro.2017.67 (2017).
- 916 6 Qiu, J. *et al.* Ubiquitination independent of E1 and E2 enzymes by bacterial
917 effectors. *Nature* **533**, 120-124, doi:10.1038/nature17657 (2016).
- 918 7 Bhogaraju, S. *et al.* Phosphoribosylation of Ubiquitin Promotes Serine
919 Ubiquitination and Impairs Conventional Ubiquitination. *Cell* **167**, 1636-1649
920 e1613, doi:10.1016/j.cell.2016.11.019 (2016).
- 921 8 Kotewicz, K. M. *et al.* A Single Legionella Effector Catalyzes a Multistep
922 Ubiquitination Pathway to Rearrange Tubular Endoplasmic Reticulum for
923 Replication. *Cell Host Microbe* **21**, 169-181, doi:10.1016/j.chom.2016.12.007
924 (2017).
- 925 9 Shin, D. *et al.* Regulation of Phosphoribosyl-Linked Serine Ubiquitination by
926 Deubiquitinases DupA and DupB. *Mol Cell* **77**, 164-179 e166,
927 doi:10.1016/j.molcel.2019.10.019 (2020).
- 928 10 Wan, M. *et al.* Deubiquitination of phosphoribosyl-ubiquitin conjugates by
929 phosphodiesterase-domain-containing Legionella effectors. *Proc Natl Acad Sci U*
930 *S A* **116**, 23518-23526, doi:10.1073/pnas.1916287116 (2019).
- 931 11 Branon, T. C. *et al.* Efficient proximity labeling in living cells and organisms with
932 TurboID. *Nat Biotechnol* **36**, 880-887, doi:10.1038/nbt.4201 (2018).
- 933 12 Voth, K. *et al.* Structural and Functional Characterization of *Legionella*
934 *pneumophila* Effector MavL. *Biomolecules* **11**, doi:10.3390/biom11121802 (2021).
- 935 13 Yan, F. *et al.* Threonine ADP-Ribosylation of Ubiquitin by a Bacterial Effector
936 Family Blocks Host Ubiquitination. *Mol Cell* **78**, 641-652 e649,
937 doi:10.1016/j.molcel.2020.03.016 (2020).
- 938 14 Tezcan-Merdol, D., Nyman, T., Lindberg, U., Haag, F., Koch-Nolte, F. & Rhen, M.
939 Actin is ADP-ribosylated by the Salmonella enterica virulence-associated protein
940 SpvB. *Mol Microbiol* **39**, 606-619, doi:10.1046/j.1365-2958.2001.02258.x (2001).
- 941 15 Fu, J., Zhou, M., Gritsenko, M. A., Nakayasu, E. S., Song, L. & Luo, Z. Q.
942 Legionella pneumophila modulates host energy metabolism by ADP-ribosylation
943 of ADP/ATP translocases. *Elife* **11**, doi:10.7554/eLife.73611 (2022).
- 944 16 Mao, Z. *et al.* SIRT6 promotes DNA repair under stress by activating PARP1.
945 *Science* **332**, 1443-1446, doi:10.1126/science.1202723 (2011).

- 946 17 Urbanus, M. L. *et al.* Diverse mechanisms of metaeffector activity in an intracellular
947 bacterial pathogen, *Legionella pneumophila*. *Mol Syst Biol* **12**, 893,
948 doi:10.15252/msb.20167381 (2016).
- 949 18 Huang, L. *et al.* The E Block motif is associated with *Legionella pneumophila*
950 translocated substrates. *Cell Microbiol* **13**, 227-245, doi:10.1111/j.1462-
951 5822.2010.01531.x (2011).
- 952 19 Liu, S., Luo, J., Zhen, X., Qiu, J., Ouyang, S. & Luo, Z. Q. Interplay between
953 bacterial deubiquitinase and ubiquitin E3 ligase regulates ubiquitin dynamics on
954 *Legionella* phagosomes. *Elife* **9**, doi:10.7554/eLife.58114 (2020).
- 955 20 Gan, N. *et al.* Regulation of phosphoribosyl ubiquitination by a calmodulin-
956 dependent glutamylase. *Nature* **572**, 387-391, doi:10.1038/s41586-019-1439-1
957 (2019).
- 958 21 Black, M. H. *et al.* Bacterial pseudokinase catalyzes protein polyglutamylation to
959 inhibit the SidE-family ubiquitin ligases. *Science* **364**, 787-792,
960 doi:10.1126/science.aaw7446 (2019).
- 961 22 Bhogaraju, S. *et al.* Inhibition of bacterial ubiquitin ligases by SidJ-calmodulin
962 catalysed glutamylation. *Nature* **572**, 382-386, doi:10.1038/s41586-019-1440-8
963 (2019).
- 964 23 Song, L. *et al.* *Legionella pneumophila* regulates host cell motility by targeting
965 Phldb2 with a 14-3-3zeta-dependent protease effector. *Elife* **11**,
966 doi:10.7554/eLife.73220 (2022).
- 967 24 Bagshaw, C. ATP analogues at a glance. *J Cell Sci* **114**, 459-460 (2001).
- 968 25 Altschul, S. F. *et al.* Gapped BLAST and PSI-BLAST: a new generation of protein
969 database search programs. *Nucleic Acids Res* **25**, 3389-3402,
970 doi:10.1093/nar/25.17.3389 (1997).
- 971 26 Zhang, D., de Souza, R. F., Anantharaman, V., Iyer, L. M. & Aravind, L.
972 Polymorphic toxin systems: Comprehensive characterization of trafficking modes,
973 processing, mechanisms of action, immunity and ecology using comparative
974 genomics. *Biol Direct* **7**, 18, doi:10.1186/1745-6150-7-18 (2012).
- 975 27 Losick, V. P., Haenssler, E., Moy, M. Y. & Isberg, R. R. LnaB: a *Legionella*
976 *pneumophila* activator of NF-kappaB. *Cell Microbiol* **12**, 1083-1097,
977 doi:10.1111/j.1462-5822.2010.01452.x (2010).
- 978 28 Casey, A. K. & Orth, K. Enzymes Involved in AMPylation and deAMPylation. *Chem*
979 *Rev* **118**, 1199-1215, doi:10.1021/acs.chemrev.7b00145 (2018).
- 980 29 Stadtman, E. R. The story of glutamine synthetase regulation. *J Biol Chem* **276**,
981 44357-44364, doi:10.1074/jbc.R100055200 (2001).
- 982 30 Muller, M. P., Peters, H., Blumer, J., Blankenfeldt, W., Goody, R. S. & Itzen, A. The
983 *Legionella* effector protein DrrA AMPylates the membrane traffic regulator Rab1b.
984 *Science* **329**, 946-949, doi:10.1126/science.1192276 (2010).
- 985 31 Xu, Y., Carr, P. D., Vasudevan, S. G. & Ollis, D. L. Structure of the adenylation
986 domain of *E. coli* glutamine synthetase adenylyl transferase: evidence for gene
987 duplication and evolution of a new active site. *J Mol Biol* **396**, 773-784,
988 doi:10.1016/j.jmb.2009.12.011 (2010).
- 989 32 Yarbrough, M. L., Li, Y., Kinch, L. N., Grishin, N. V., Ball, H. L. & Orth, K.
990 AMPylation of Rho GTPases by *Vibrio* VopS disrupts effector binding and
991 downstream signaling. *Science* **323**, 269-272, doi:10.1126/science.1166382
992 (2009).

- 993 33 Sreelatha, A. *et al.* Protein AMPylation by an Evolutionarily Conserved
994 Pseudokinase. *Cell* **175**, 809-821 e819, doi:10.1016/j.cell.2018.08.046 (2018).
- 995 34 Tan, Y., Arnold, R. J. & Luo, Z. Q. Legionella pneumophila regulates the small
996 GTPase Rab1 activity by reversible phosphorylation. *Proc Natl Acad Sci U*
997 *S A* **108**, 21212-21217, doi:10.1073/pnas.1114023109 (2011).
- 998 35 Feng, F. *et al.* A Xanthomonas uridine 5'-monophosphate transferase inhibits plant
999 immune kinases. *Nature* **485**, 114-118, doi:10.1038/nature10962 (2012).
- 1000 36 Casey, A. K. *et al.* Fic-mediated AMPylation tempers the unfolded protein
1001 response during physiological stress. *Proc Natl Acad Sci U S A* **119**, e2208317119,
1002 doi:10.1073/pnas.2208317119 (2022).
- 1003 37 Tan, Y. & Luo, Z. Q. Legionella pneumophila SidD is a deAMPyase that modifies
1004 Rab1. *Nature* **475**, 506-509, doi:10.1038/nature10307 (2011).
- 1005 38 Preissler, S., Rato, C., Perera, L., Saudek, V. & Ron, D. FICD acts bifunctionally
1006 to AMPylate and de-AMPyate the endoplasmic reticulum chaperone BiP. *Nat*
1007 *Struct Mol Biol* **24**, 23-29, doi:10.1038/nsmb.3337 (2017).
- 1008 39 Drum, C. L. *et al.* Structural basis for the activation of anthrax adenylyl cyclase
1009 exotoxin by calmodulin. *Nature* **415**, 396-402, doi:10.1038/415396a (2002).
- 1010 40 Guo, Q., Shen, Y., Lee, Y. S., Gibbs, C. S., Mrksich, M. & Tang, W. J. Structural
1011 basis for the interaction of Bordetella pertussis adenylyl cyclase toxin with
1012 calmodulin. *EMBO J* **24**, 3190-3201, doi:10.1038/sj.emboj.7600800 (2005).
- 1013 41 Berger, K. H. & Isberg, R. R. Two distinct defects in intracellular growth
1014 complemented by a single genetic locus in Legionella pneumophila. *Mol Microbiol*
1015 **7**, 7-19, doi:10.1111/j.1365-2958.1993.tb01092.x (1993).
- 1016 42 Luo, Z. Q. & Isberg, R. R. Multiple substrates of the Legionella pneumophila
1017 Dot/Icm system identified by interbacterial protein transfer. *Proc Natl Acad Sci U*
1018 *S A* **101**, 841-846, doi:10.1073/pnas.0304916101 (2004).
- 1019 43 Xu, L., Shen, X., Bryan, A., Banga, S., Swanson, M. S. & Luo, Z. Q. Inhibition of
1020 host vacuolar H⁺-ATPase activity by a Legionella pneumophila effector. *PLoS*
1021 *Pathog* **6**, e1000822, doi:10.1371/journal.ppat.1000822 (2010).
- 1022 44 Gan, N. *et al.* Legionella pneumophila regulates the activity of UBE2N by
1023 deamidase-mediated deubiquitination. *EMBO J* **39**, e102806,
1024 doi:10.15252/embj.2019102806 (2020).
- 1025 45 Song, L. *et al.* The Legionella Effector SdjA Is a Bifunctional Enzyme That
1026 Distinctly Regulates Phosphoribosyl Ubiquitination. *mBio*, e0231621,
1027 doi:10.1128/mBio.02316-21 (2021).
- 1028 46 Fan, H. Y., Cheng, K. K. & Klein, H. L. Mutations in the RNA polymerase II
1029 transcription machinery suppress the hyperrecombination mutant hpr1 delta of
1030 *Saccharomyces cerevisiae*. *Genetics* **142**, 749-759,
1031 doi:10.1093/genetics/142.3.749 (1996).
- 1032 47 Schuck, P. Size-distribution analysis of macromolecules by sedimentation velocity
1033 ultracentrifugation and lamm equation modeling. *Biophys J* **78**, 1606-1619,
1034 doi:10.1016/S0006-3495(00)76713-0 (2000).
- 1035 48 Philo, J. S. SEDNTERP: a calculation and database utility to aid interpretation of
1036 analytical ultracentrifugation and light scattering data. *Eur Biophys J* **52**, 233-266,
1037 doi:10.1007/s00249-023-01629-0 (2023).
- 1038 49 Hsu, F. *et al.* The Legionella effector SidC defines a unique family of ubiquitin
1039 ligases important for bacterial phagosomal remodeling. *Proc Natl Acad Sci U S A*
1040 **111**, 10538-10543, doi:10.1073/pnas.1402605111 (2014).

1041 50 Shevchenko, A., Tomas, H., Havlis, J., Olsen, J. V. & Mann, M. In-gel digestion for
1042 mass spectrometric characterization of proteins and proteomes. *Nat Protoc* **1**,
1043 2856-2860, doi:10.1038/nprot.2006.468 (2006).

1044 51 Jumper, J. *et al.* Highly accurate protein structure prediction with AlphaFold.
1045 *Nature* **596**, 583-589, doi:10.1038/s41586-021-03819-2 (2021).

1046 52 Adams, P. D. *et al.* PHENIX: building new software for automated crystallographic
1047 structure determination. *Acta Crystallogr D Biol Crystallogr* **58**, 1948-1954,
1048 doi:10.1107/s0907444902016657 (2002).

1049 53 Katoh, K. & Standley, D. M. MAFFT multiple sequence alignment software version
1050 7: improvements in performance and usability. *Mol Biol Evol* **30**, 772-780,
1051 doi:10.1093/molbev/mst010 (2013).

1052 54 Nguyen, L. T., Schmidt, H. A., von Haeseler, A. & Minh, B. Q. IQ-TREE: a fast and
1053 effective stochastic algorithm for estimating maximum-likelihood phylogenies. *Mol*
1054 *Biol Evol* **32**, 268-274, doi:10.1093/molbev/msu300 (2015).

1055 55 Kalyaanamoorthy, S., Minh, B. Q., Wong, T. K. F., von Haeseler, A. & Jermini, L.
1056 S. ModelFinder: fast model selection for accurate phylogenetic estimates. *Nat*
1057 *Methods* **14**, 587-589, doi:10.1038/nmeth.4285 (2017).

1058 56 Letunic, I. & Bork, P. Interactive Tree Of Life (iTOL) v5: an online tool for
1059 phylogenetic tree display and annotation. *Nucleic Acids Res* **49**, W293-W296,
1060 doi:10.1093/nar/gkab301 (2021).

1061 57 Gaussian09, R. A. 1, MJ Frisch, GW Trucks, HB Schlegel, GE Scuseria, MA Robb,
1062 JR Cheeseman, G. Scalmani, V. Barone, B. Mennucci, GA Petersson *et al.*,
1063 Gaussian. *Inc.*, Wallingford CT (2009).

1064 58 Morris, G. M. *et al.* AutoDock4 and AutoDockTools4: Automated docking with
1065 selective receptor flexibility. *Journal of computational chemistry* **30**, 2785-2791
1066 (2009).

1067 59 Morris, G. M. *et al.* Automated docking using a Lamarckian genetic algorithm and
1068 an empirical binding free energy function. *Journal of computational chemistry* **19**,
1069 1639-1662 (1998).

1070

Figures

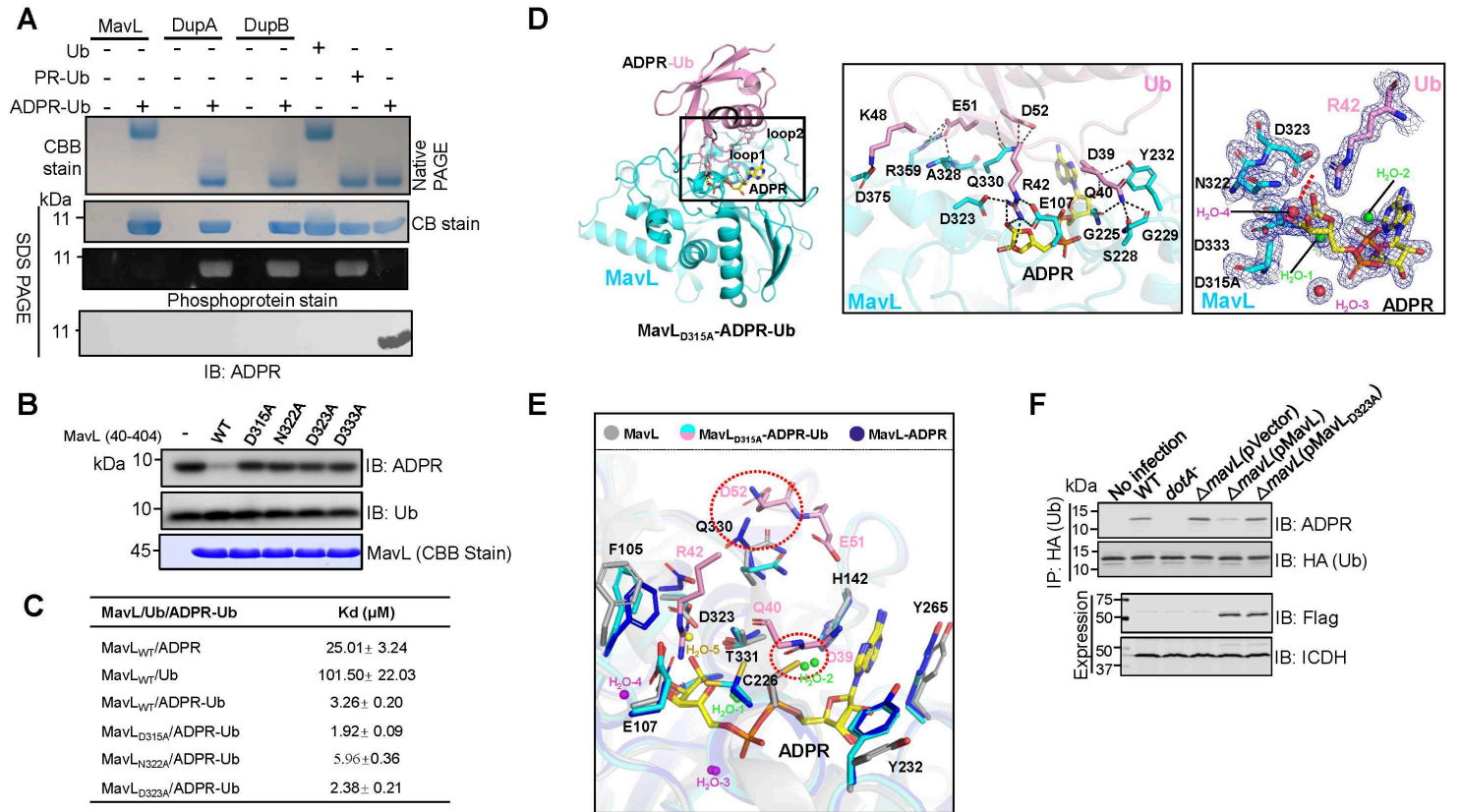


Figure 1

MavL is a macro domain protein that converts ADPR-Ub into ADP-ribose and ubiquitin a. Hydrolysis of ADPR-Ub into ADPR and Ub by MavL DupA or DupB. Recombinant proteins were incubated with ADPR-Ub and the production of native Ub was detected by native polyacrylamide gel electrophoresis (upper panel). Native Ub, PR-Ub and ADPR- Ub were loaded separately as controls. Identical samples separated by SDS-PAGE were detected by CBB staining, phosphoprotein stain or immunoblotting with an ADPR-specific antibody (lower three panels). b. Mutational analysis of residues important for the de-ADP ribosylation activity of MavL. Recombinant MavL or its mutants were incubated with ADPR-Ub and the reduction of the reactant was detected by immunoblotting with an ADPR-specific antibody. c. Binding of Ub, ADPR-Ub and ADPR to MavL40-404 or its mutants. Binding affinity was evaluated using a low volume Nano ITC set at 20°C. d. Ribbon diagram representation of the MavL(40-404)D315A-ADPR-Ub complex. Ub, ADPR and MavL are colored in pink, yellow and cyan, respectively. The recognition of ADPR- Ub by MavL as well as the interactions between the two proteins are shown in the middle panel. The 2mFo-DFc(blue) and mFo-DFc (green) electron-density maps of the key residues of MavL, Ub and water surrounding ribose involved in forming the catalytic center are contoured at the 1.5 σ and 3.0 σ levels and shown in the right panel. It represents the transient state of the substrate catalyzed by MavL. The N-glycosidic bond between the side chain of R42 in Ub and the ADPR moiety was cleaved, as indicated by the red dashed lines and arrow. e. The overall structure of MavL(40-404)D315A-ADPR-Ub and its comparison to Apo MavL (gray) and MavL-ADPR (blue). The conformational changes that contribute to

the opening of the catalytic pocket to facilitate the binding of ADPR-Ub and the subsequent reaction were shown. Residues that cause steric hindrance between Apo MavL and Ub were marked with red dashed circles. f. MavL reduces the level of ADPR-Ub in infected cells. The indicated *L. pneumophila* strains were used to infected cells expressing 3xHA-Ub and the accumulation of ADPR-Ub was detected after HA antibody immunoprecipitation. Expression of Flag-MavL and its mutant was detected with Flag antibody and isocitrate dehydrogenase (ICDH) was probed as a loading control.

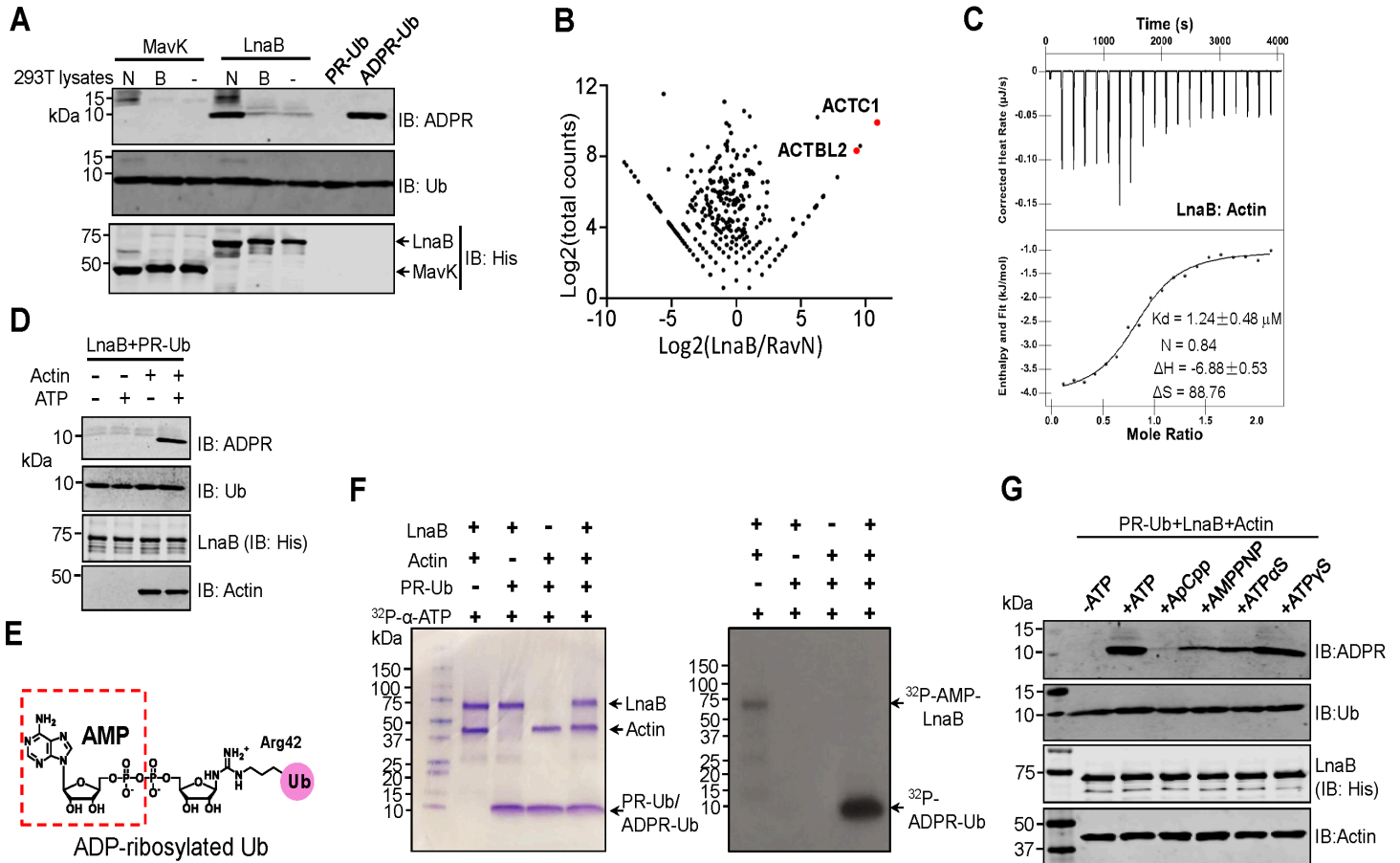


Figure 2

Conversion of PR-Ub into ADPR-Ub by LnaB requires Actin as a co-factor a. Native lysates of mammalian cells activate LnaB. Native (N) or boiled (B) lysates of 293HEK cells were added to reactions containing PR-Ub, MavK or LnaB and the production of ADPR-Ub was detected by immunoblotting. b. Identification of Actin as a LnaB-binding protein. Flag-LnaB expressed in HEK293T cells was isolated by immunoprecipitation and the bound proteins were identified by mass spectrometry. Similarly obtained samples with Flag-RavN were used as a control. alpha Actin (ACTC1) and beta Actin-like 2 (ACTBL2) were the among the most abundant proteins identified. c. Interactions between LnaB and Actin measured by ITC. Raw ITC curves (top panel) and binding isotherms with fitting curves (bottom panel) of LnaB titration by Actin. The thermogram is a monophasic curve with an inflection point at molar ratio of 0.84. The binding affinity is approximately 1.24 μ M and the stoichiometry is 1:1 of Actin:LnaB. The thermodynamic parameters were also shown, ΔH : -6.88 $\text{kJ}\cdot\text{mol}^{-1}$ and ΔS : 88.75 $\text{J}\cdot\text{mol}^{-1}\cdot\text{K}^{-1}$. d. LnaB and actin utilize ATP to convert PR-Ub into ADPR-Ub. Actin was added to a subset of reactions

containing LnaB and PR-Ub. Samples separated by SDS-PAGE were probed for ADPR-Ub (upper panel), ubiquitin, LnaB or Actin by immunoblotting with antibodies specific for each protein or its epitope tag. e-f. LnaB transfers the AMP moiety of ATP to PR-Ub. The chemical structure of ADPR-Ub with the AMP moiety added to phosphate group on PR-Ub being highlighted (dashed box) (e). 32 P- α -ATP was added to the indicated reactions and incubated at 37°C for 1 h. Samples separated by SDS-PAGE were detected by CBB staining (left) and autoradiograph, respectively. Note the presence of self-modified LnaB in the reaction without PR-Ub (f). g. ATP analogs with a cleavable α phosphate support LnaB activity. Samples of reactions receiving the indicated ATP analogs were resolved by SDS-PAGE, and ADPR-Ub and the reactants were detected by immunoblotting by antibodies specific for ADPR, Ub, LnaB or Actin. Note that ApCpp is uncleavable at the α position thus did not support the activity of LnaB. In each case, similar results were obtained in at least three independent experiments

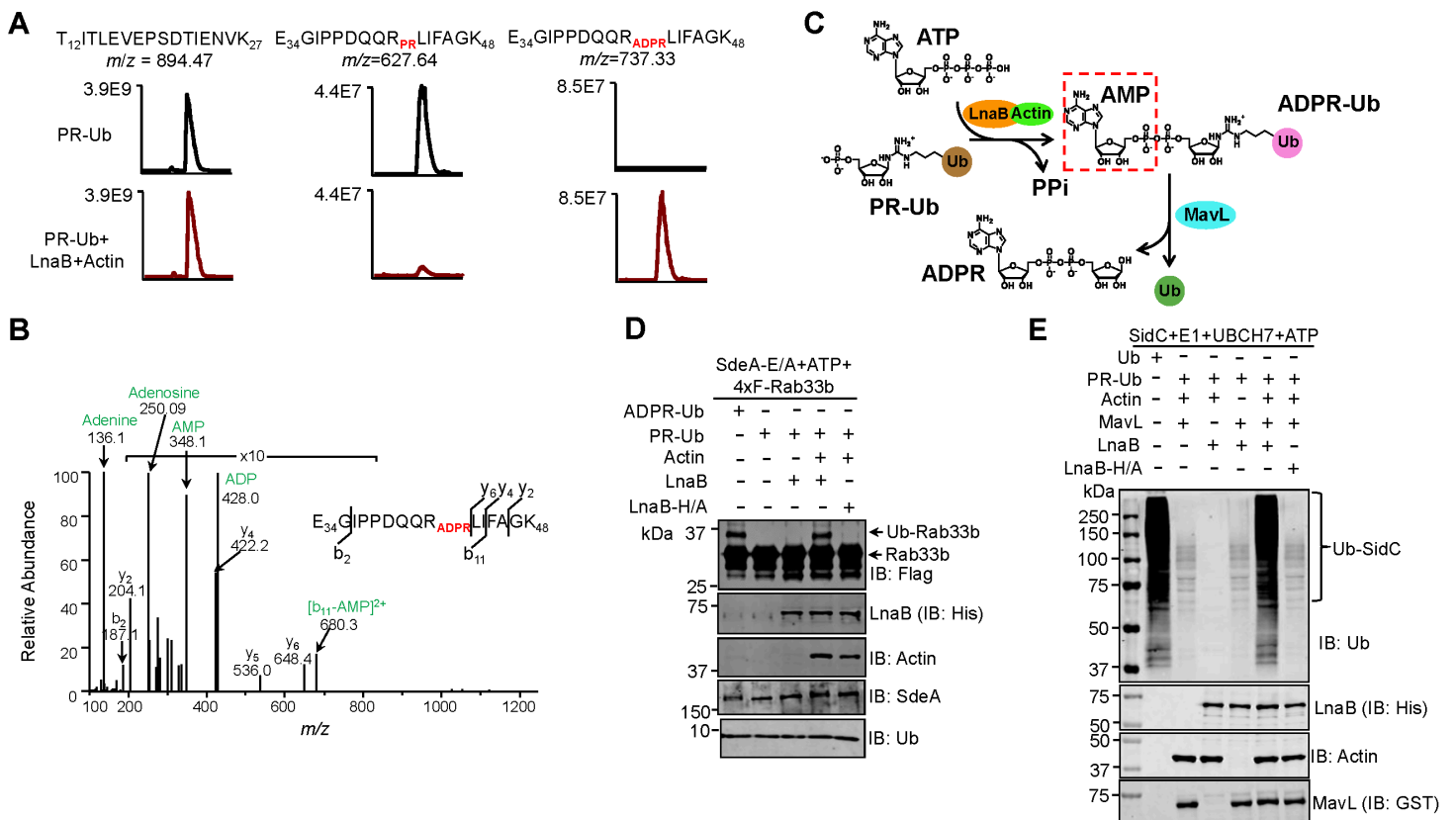


Figure 3

LnaB and MavL sequentially convert PR-Ub into ADPR and active ubiquitin a-b. Detection of LnaB-mediated conversion of PR-Ub into ADPR-Ub by mass spectrometric analysis. Excised protein bands from SDS-PAGE gels corresponding to PR-Ub prior to the reaction or ADPR-Ub after incubated with ATP, LnaB and Actin were digested with trypsin and analyzed by mass spectrometry. A reference fragment T12ITLEVEPSDTIENVK₂₇ was present in both samples with similar abundance (a left panel). The abundance of the fragment with PR-modified R42 was high in the PR-Ub samples but became almost undetectable after reaction with LnaB, ATP and Actin, which was accompanied by the increase of ADPR-modified fragment. A MS/MS spectrum indicating ADPR modification of R42 was shown in b. c. A reaction scheme depicting the conversion of PR-Ub into ubiquitin by LnaB and MavL. The AMPylation

activity of LnaB first converts PR-Ub into ADPR-Ub, which is further reduced into ADP-ribose and ubiquitin by MavL. The AMP moiety defined by a dash line rectangle indicates the chemical group added to PR-Ub by LnaB. d. The use of ADPR-Ub produced from PR-Ub by LnaB in protein modification by the phosphodiesterase (PDE) activity of SdeA. PR-Ub was incubated in the indicated reactions and the ability to ubiquitinate Rab33b was detected by the formation of higher MW species detected by immunoblotting with the Flag-specific antibody. Native ADPR-Ub was included as a control (1st lane). e. Conventional ubiquitination by ubiquitin produced by MavL and LnaB from PR-Ub. A series of reactions containing PR-Ub and combinations of relevant proteins were allowed to proceed for 1 h at 37°C. The products were boiled for 5 min at 95°C and a cocktail containing E1, E2, SidC (E3) and ATP was added, self-ubiquitination of SidC was detected by immunoblotting with a ubiquitin-specific antibody.

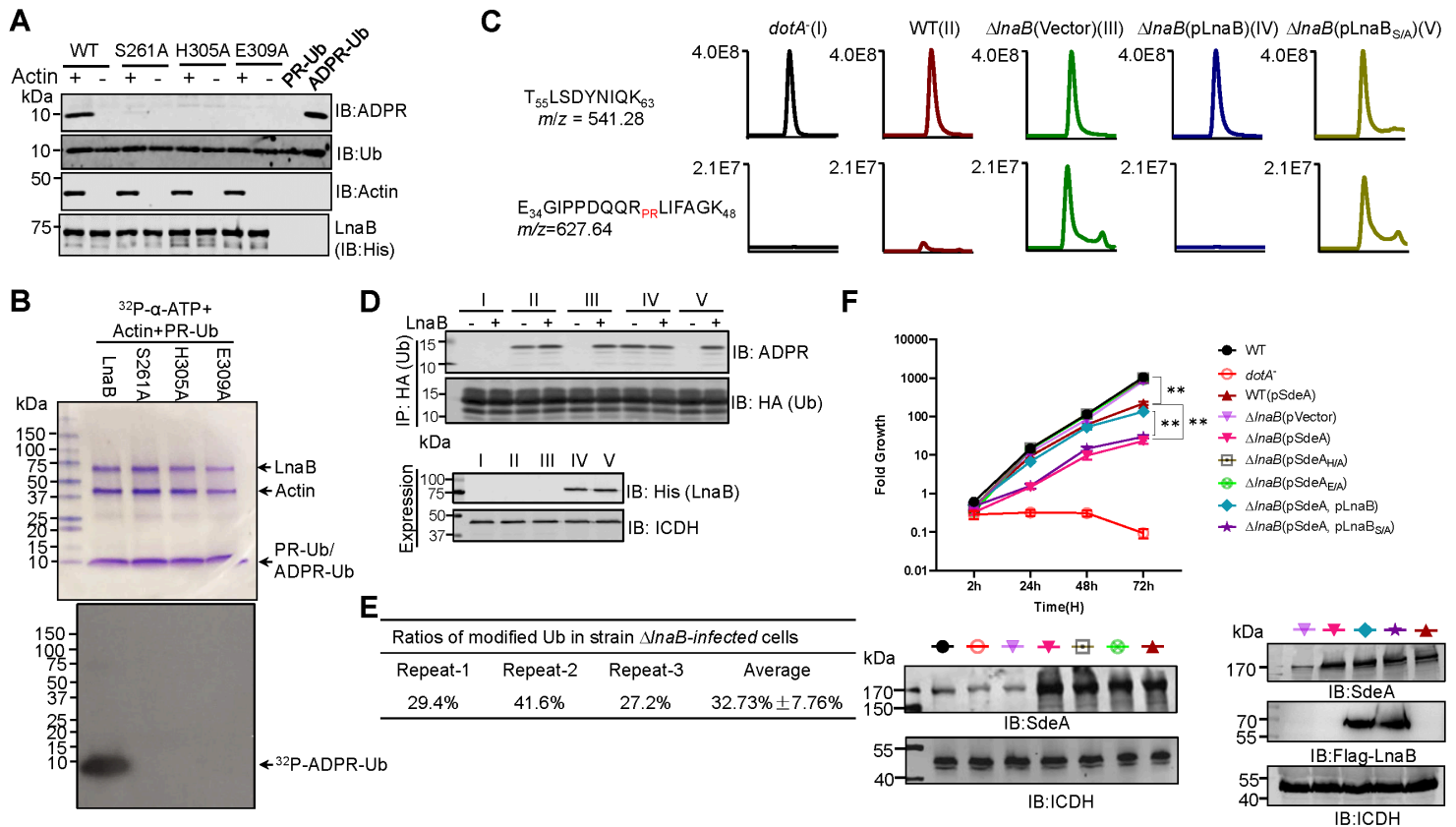


Figure 4

The reaction catalyzed by LnaB required an S-HxxxE motif a-b. Conversion of PR-Ub into ADPR-Ub by LnaB requires an S-HxxxE motif. Samples of reactions containing ATP, PR-Ub, LnaB, Actin, LnaB or its mutants and resolved by SDS-PAGE were detected for the production of ADPR-Ub (top). Each reactant was detected by immunoblotting with the appropriate antibodies (a). Similar reactions with 32 P- α -ATP were established, proteins were detected by CBB staining (upper) and the production of 32 P-ADPR-Ub was detected by autoradiograph (lower) (b). c-d. LnaB functions to convert PR-Ub into ADPR-Ub in cells infected with *L. pneumophila*. HEK293 cells transfected to express 3xHA-Ub were infected with the indicated bacterial strains (I to V). Immunoprecipitation products obtained by HA antibody from lysates of infected cells were analyzed by mass spectrometry to detect differently modified ubiquitin (c). Recombinant LnaB was added to a subset of similar prepared lysates of infected cells and the

accumulation of PR-Ub was assessed by detecting LnaB-mediated ADPR-Ub production (d). e. The ratio of modified ubiquitin (PR-Ub) in cells infected with the Δ LnaB mutant. Cells expressing HA-ubiquitin was infected with strain Lp02 Δ LnaB for 2 h. HA-ubiquitin isolated by immunoprecipitation was analyzed by mass spectrometry to determine the ratio of modified ubiquitin. f. Overexpression of SdeA in the Δ LnaB mutant affects intracellular bacterial growth. *D. discoideum* was infected with the indicated *L. pneumophila* strains and the growth of the bacteria was evaluated. Note that strain Δ LnaB(pSdeA) displayed significant defects in intracellular growth (upper panel). The expression of SdeA in the testing strains was probed by immunoblotting (lower panel). Data shown were one representative of three independent experiments done in triplicate with similar results.

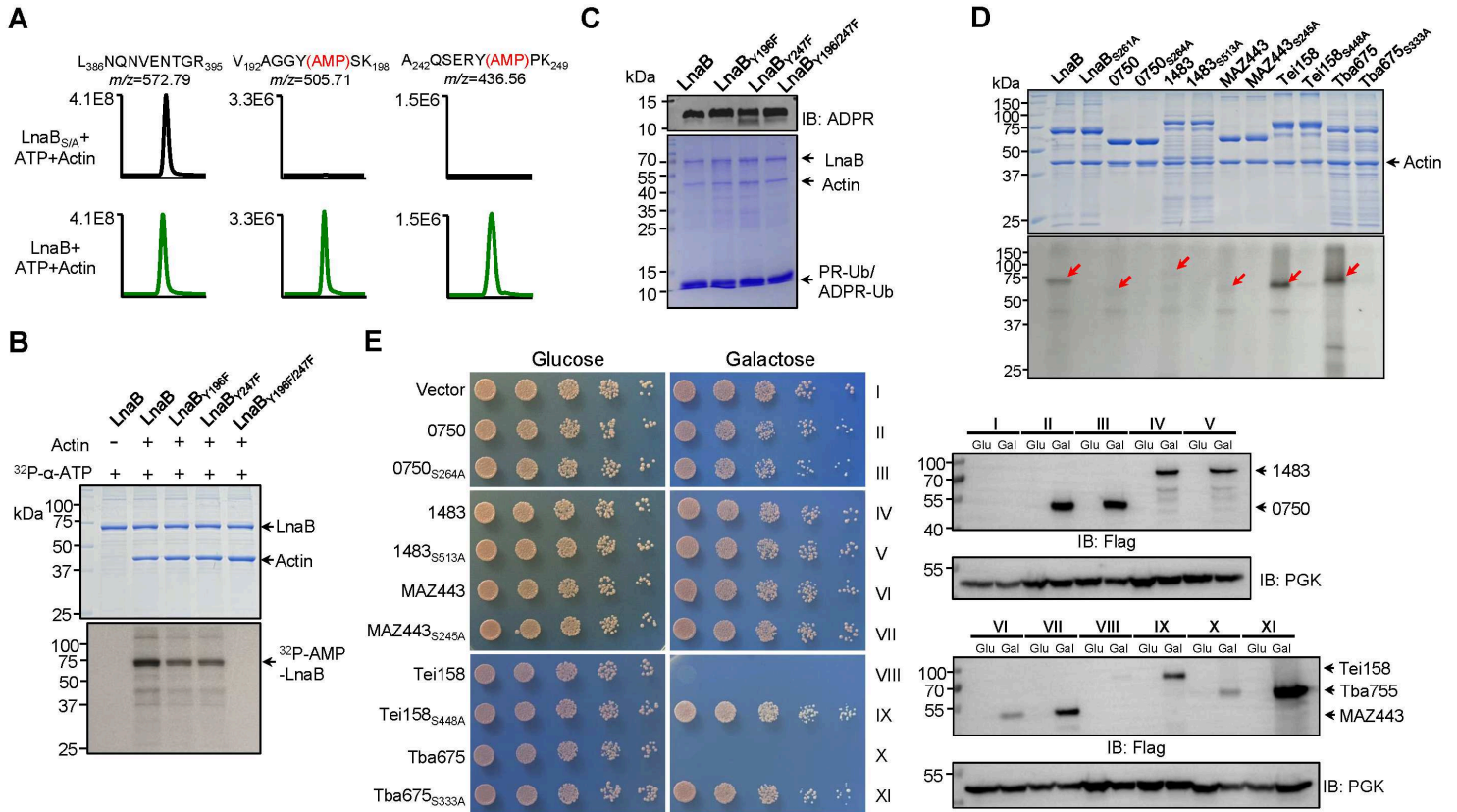


Figure 5

Self-AMPylation activity of members of the S-HxxxE toxin family a. LnaB self-AMPylates at Y196 and Y247. Protein bands corresponding to LnaB from the indicated reactions were analyzed to identify the modified residues by mass spectrometry. b-c. Mutations of the AMPylated Tyr residues abolished the activity of LnaB. LnaB or its mutants was incubated with ^{32}P - α -ATP and Actin and production of self-modified protein was detected by autoradiograph (b). Similar reactions receiving PR-Ub were established to probe the impact of the mutations on the conversion of PR-Ub into ADPR-Ub, which was detected by immunoblotting (top) and the proteins in the reactions were detected by CBB staining (lower). d. Self-AMPylation by members of the S-HxxxE family. Recombinant proteins of the indicated toxins were incubated with ^{32}P - α -ATP and Actin. Samples resolved by SDS-PAGE were detected for AMPylation by autoradiograph (lower) and for the proteins by CBB staining (upper). Red arrows indicated AMPylated proteins. Note that in each case, self-AMPylation required an intact S-HxxxE motif. e. Yeast toxicity by

the toxins required an intact S-HXXXE motif. Serially diluted cells of yeast strains expressing the indicated toxin genes or their S-HxxxE mutants were spotted on medium containing glucose or galactose. Images were acquired after 3-day incubation at 30°C (left). The expression of the proteins was probed by immunoblotting with the Flag- specific antibody. The phosphoglycerate kinase (PGK) was probed as a loading control.

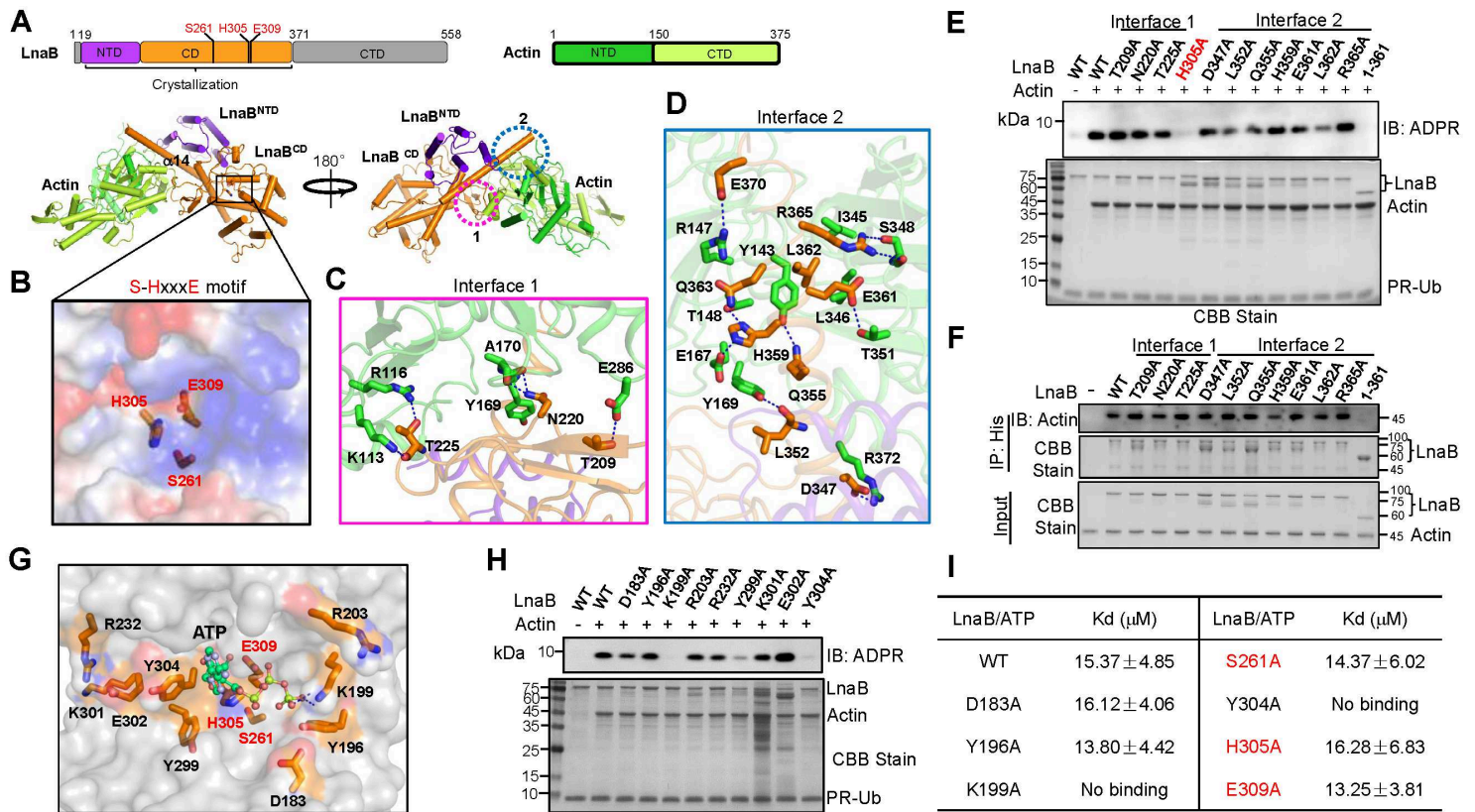


Figure 6

LnaB-Actin binary complex structure reveals a unique catalytic mechanism on AMPylation. a. Cylindrical cartoon diagram representation of the LnaB-Actin complex. The top panels represent schematic diagrams of the regions for domain organization of LnaB and Actin. LnaB consists of the N-terminal domain (NTD, purple), the catalytic domain (CD, orange) and the C-terminal domain (CTD, grey); Actin is composed of NTD (green) and CTD (Limon). S261, H305 and E309 of the S-HxxxE motif are shown in red. The bottom panel shows the LnaB-Actin binary structure. Domains of LnaB and Actin were colored in accordance with the diagrams (top). The interfaces involved in LnaB-Actin interactions were highlighted in two dashed line circles. b. S261, H305 and E309 formed a platform in the structure of LnaB. Residues were represented as sticks and LnaB was depicted in surface, colored according to the electrostatic surface potential [contoured from -6kBT (red) to +6kBT (blue)]. c-d. The interfaces involved in LnaB-Actin interactions. LnaB and Actin were shown as orange and green cartoons, respectively. Residues important for binding were shown as sticks (Actin in green and LnaB in orange). Hydrogen bonds were marked by blue dashed lines. e. Optimal binding to Actin is required for maximal activity of LnaB. Indicated LnaB mutants were individually incubated with Actin, ATP, and PR-Ub for 30 min at 37°C and their activity in converting PR-Ub into ADPR-Ub was evaluated by immunoblotting with an ADPR-

specific antibody. Proteins in the reactions were detected by CBB staining. f. Evaluation of the binding of Actin to LnaB and its mutants by Ni²⁺ beads pulldown. His₆- LnaB and its mutants were individually incubated with Actin at 40 C for 6 h prior to pulldown with Ni²⁺ beads. Actin was detected using anti-Actin antibodies and proteins were detected by CBB staining. g-i. An ATP-binding pocket in LnaB identified by molecular docking. LnaB was displayed in a grey surface model. Residues potentially involved in binding ATP was indicated as orange sticks. ATP was shown as a cyan stick-ball model and hydrogen bonds were represented by blue dashed lines (G). LnaB mutants were evaluated for the ability to convert PR-Ub into ADPR-Ub with reactions described above. Proteins were detected by CBB staining (H). The affinity between ATP and LnaB and its mutants was determined using isothermal titration calorimetry (ITC). The binding constant (K_d) was calculated by the NanoAnalyze software package. Data shown are one representative of three independent experiments with similar results (E, F, H and I).

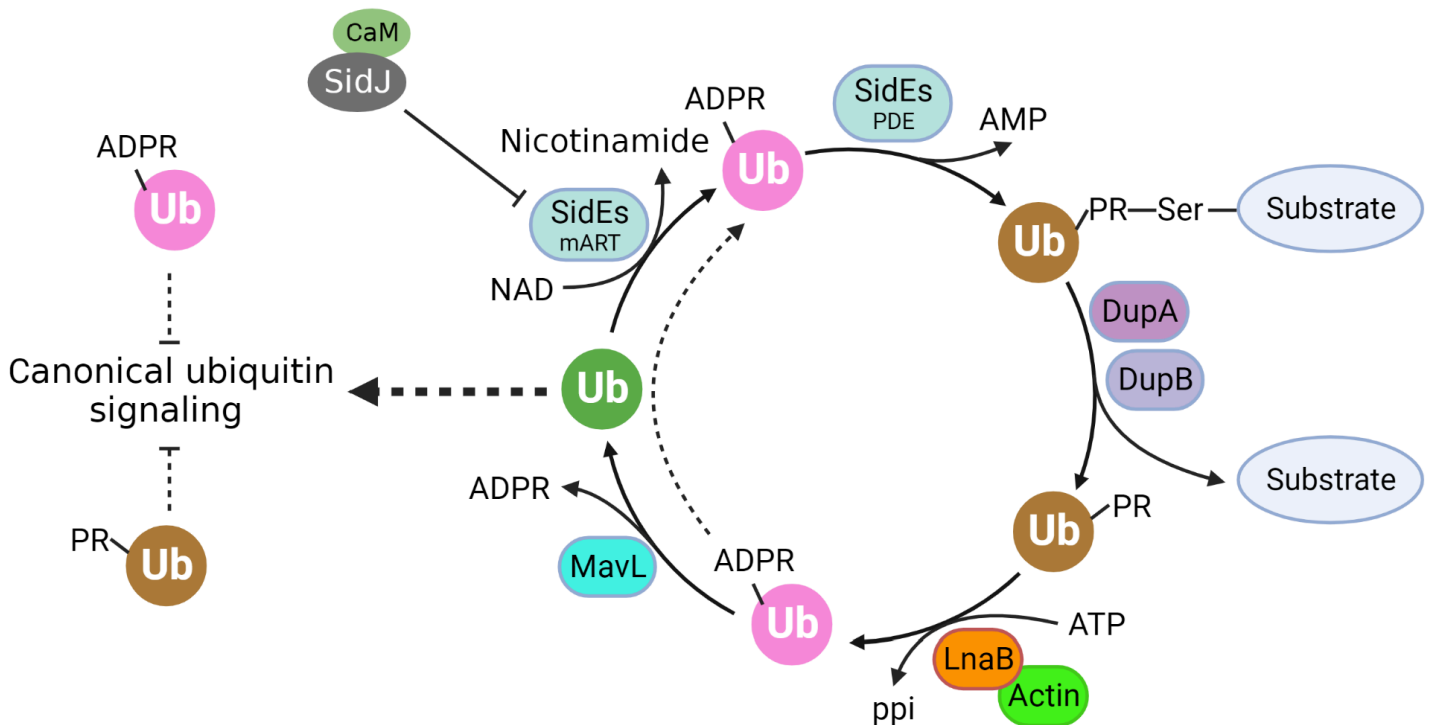


Figure 7

The cycling of ubiquitin by Dot/Icm effectors in cells infected by *L. pneumophila*. Ubiquitin is converted into ADPR-Ub by the mART activity of SidEs, which is used to modified proteins by phosphoribosyl ubiquitination. The reversal of the modification produced PR-Ub, which is converted into native ubiquitin by sequential reactions catalyzed by LnaB and MavL. Note that both ADPR-Ub and PR-Ub may interfere with canonical ubiquitin signaling and that ADPR-Ub produced from PR-Ub by LnaB may be used by the PDE activity of SidEs for protein modification.

Supplementary Files

This is a list of supplementary files associated with this preprint. Click to download.

- [LnaBinteractingproteins.xlsx](#)
- [8IPJMavLADPRUbValidationreport.pdf](#)
- [8IPWMavLADPRValidationreport.pdf](#)
- [8J9Bvalreportfullupdated.pdf](#)
- [Editorialpolicychecklist1.pdf](#)
- [FuetalSupplementaryinformation.pdf](#)
- [Reportingsummary1.pdf](#)
- [UncroppedimagingNC.pdf](#)